Design and Development of a Novel Liquid Desiccant Air-Conditioning System

by

Ross A. Bonner

Submitted to the Department of Mechanical Engineering
in partial fulfillment of the requirements for the degree of

Master of Science in Mechanical Engineering

at the

MASSACHUSETTS INSTITUTE OF TECHNOLOGY

September 2020

© Massachusetts Institute of Technology 2020. All rights reserved.

Author . . . .
Department of Mechanical Engineering
September 16, 2020

Certified by. . . . .
Douglas Hart
Professor
Thesis Supervisor

Accepted by . . . .
Nicolas Hadjiconstantinou
Chairman, Department Committee on Graduate Theses

Design and Development of a Novel Liquid Desiccant Air-Conditioning System

by

Ross A. Bonner

Submitted to the Department of Mechanical Engineering
on September 16, 2020, in partial fulfillment of the
requirements for the degree of
Master of Science in Mechanical Engineering

Abstract

The Direct Evaporative Closed Air Loop (DECAL) system is a novel high efficiency liquid desiccant air-conditioning (LDAC) system which runs primarily on thermal energy rather than electricity. It is designed for residential cooling in hot and humid climates where demand is growing rapidly and incumbent direct-expansion system performance is poor. Unlike other LDAC systems, DECAL is modular. This allows the indoor hardware to remain small and non-intrusive, and offers increased flexibility to install the system in existing building stock without costly changes to the structure.

This work lays out the basic operating cycle of the DECAL system and shows its thermodynamic merits in terms of ideal system performance against other LDAC systems. Design studies show DECAL offers improved thermal efficiency, especially in humid climates. The ideal thermal coefficient of performance (COP_{th}) is 1.24 at the design point ambient condition of 35C, 60% RH. A mathematical model is built to better characterize performance and optimize the system design. With transport inefficiencies included, the optimal system electrical and thermal COP (COP_e and COP_{th}) are 46.3 and 0.759 respectively for a LiCl system at the design point. These results show the DECAL system could reduce electrical consumption by over 85% from present day best-in-class systems using low-grade thermal energy.

A benchtop scaled test of the closed air loop is constructed to validate the model. Experimental test results agree well with the model predictions for evaporative cooling effectiveness and sensible heat exchange, as well as pressure drop. The drying effect of the LAMEE is lower than anticipated. This is likely due to crystallization of liquid desiccant in the pores of the membrane, resulting in a high vapor diffusion resistance. Adjusting for this effect, full system test measurements match the system model well. The benchtop rig testing verified that the closed air loop is capable of generating a sensible cooling effect, but further testing is required to demonstrate modelled figures of merit are achievable.

Thesis Supervisor: Douglas Hart
Title: Professor

Acknowledgments

This work sits atop a mountain of support, patience, and passion from an outstanding network of people. I owe each of you an enormous debt of gratitude and hope I'm able to pay forward your generosity and good will.

Julie - there are no words to express how grateful I am for everything you've done to make this possible. I find myself beginning to write one of those "gee, thanks for putting up with me!" aww shucks style thank you notes but that doesn't begin to capture it. You really sacrificed for this, and in the end this is as much your accomplishment as it is mine. I hope you feel that. I know long nights for me are long nights for you, and my focus on this has stolen a lot of moments we could have shared. Going forward I'm going to make time to live in the moment and keep reminding you that every little thing is gonna be alright.

Mom - thank you for showing me through your example the importance of love, patience, and selflessness in service of others. You would be surprised how often your voice pops in my head to remind me not to "cut the head off" when I'm at risk of messing up a good thing because it isn't quite perfect.

Dad - you taught me that great things come through hard work and just a pinch of stubbornness. Because of you I know the value of keeping myself above reproach and making sure the job is done right before putting my name on it.

Doug and Peter - thank you for introducing me to the challenge of low carbon cooling back in 2.013, and for sparking a real passion in me that has pushed me to expand my horizons to make the world a better place.

To GE aviation and all my friends at GE - thank you for sponsoring my tuition at MIT and nurturing my growth as an engineer through the Edison program and beyond. Special thanks to Tyler Hooper, Phil Weed, Paul Patoulidis, Rob Brown, Alan Grissino, and Don Desander who mentored me throughout my time at GE.

Alex - thanks for being there for me throughout ASP so I wasn't going it alone. You gave me a place to park near Kendall, a friendly face to de-stress with at the Muddy after a long week, and most importantly you always made me look good by

showing up just slightly later than I did!

Leslie Regan - thanks for going out of your way (several times) to go to bat for me when I fell short on administrative tasks and deadlines 101. Having such a staunch advocate in the department always made MIT feel like home.

Sorin and Matt - thanks for seeing potential in me and giving me a platform to take the climate-change-fighting spirit from my thesis work and apply it in the startup world. I can't wait to help make great things happen with Transaera.

Contents

List of Figures

List of Tables

Chapter 1

Introduction

This work details the design and development of an energy-efficient air conditioning system which runs primarily on low-grade heat. The aim of this research is to fill the growing need for human cooling without further contributing to climate change. To achieve this goal, a step-change improvement in efficiency is needed in the near future. This chapter establishes the urgent need for high-efficiency air conditioning, reviews some of the pertinent principles, and summarizes the state of the art and recent advances in the literature.

1.0.1 Climate Change

Climate change presents a challenge of unprecedented scale, and the window to avoid the most severe consequences is extremely narrow. The actions we take now could make the difference between 1.5C warming and 2C warming, and the difference between these two scenarios is dramatic. In broad terms, to achieve 1.5C warming, we must reduce net CO2 emissions by 45% from 2010 levels by 2030, and achieve net zero by 2050. 2C pathways correspond to 25% reduction by 2030 and net zero in 2070. This reduction requires annual investment in low-carbon technology and energy efficiency to increase sixfold by 2050 [25].

The International Energy Agency (IEA) lays out two scenarios to illustrate the changes possible through intelligent energy policy and technology. The "Current Poli-

cies" scenario which assumes business as usual, and the "Sustainable Development" scenario which avoids the worst consequences of global warming, and supports the United Nations Sustainable Development Goals (SDGs), including universal access to modern energy by 2030 (SDG 7). Dramatic increases in energy efficiency are at the heart of the Sustainable Development scenario, and our current trend is not improving fast enough. [4] The IPCC states mitigation ambitions in the Paris Agreement are not sufficient to limit global warming to 1.5C. Even if scaled up significantly after 2030, global emissions must begin to decline well before 2030. [25] The IEA Sustainable Development scenario reaches carbon neutral around 2070, but does not meet 1.5C without use of carbon capture and sequestration (CCS). [4]

Global mean surface temperature (GSMT) has already risen around 1C above pre-industrial levels, and is increasing at a rate of 0.2C per decade. Depending on the method of approximation, the remaining budget to achieve a 50% probability of remaining under 1.5C warming is between 580 and 770 $GtCO_2$, with the difference primarily being the treatment of Earth system feedbacks such as the thawing of permafrost. [25]

Our collective leverage to bend the energy curve down is strongest now and only gets weaker over time, so the time is now to reduce our energy demand through innovation.

1.1   Growing Demand for Space Cooling

According to the IEA, the increasing demand for space cooling is "one of the most critical blind spots in today's energy debate". Use of air conditioners and electric fans to cool an occupied space (collectively referred to as space cooling) accounts for around 20% of total electricity used in buildings worldwide. Energy use for space cooling has more than tripled between 1990 and 2016, with unit sales quadrupling up to 135 million units in the same time frame. Space cooling is the fastest growing end use of energy in buildings. [3]
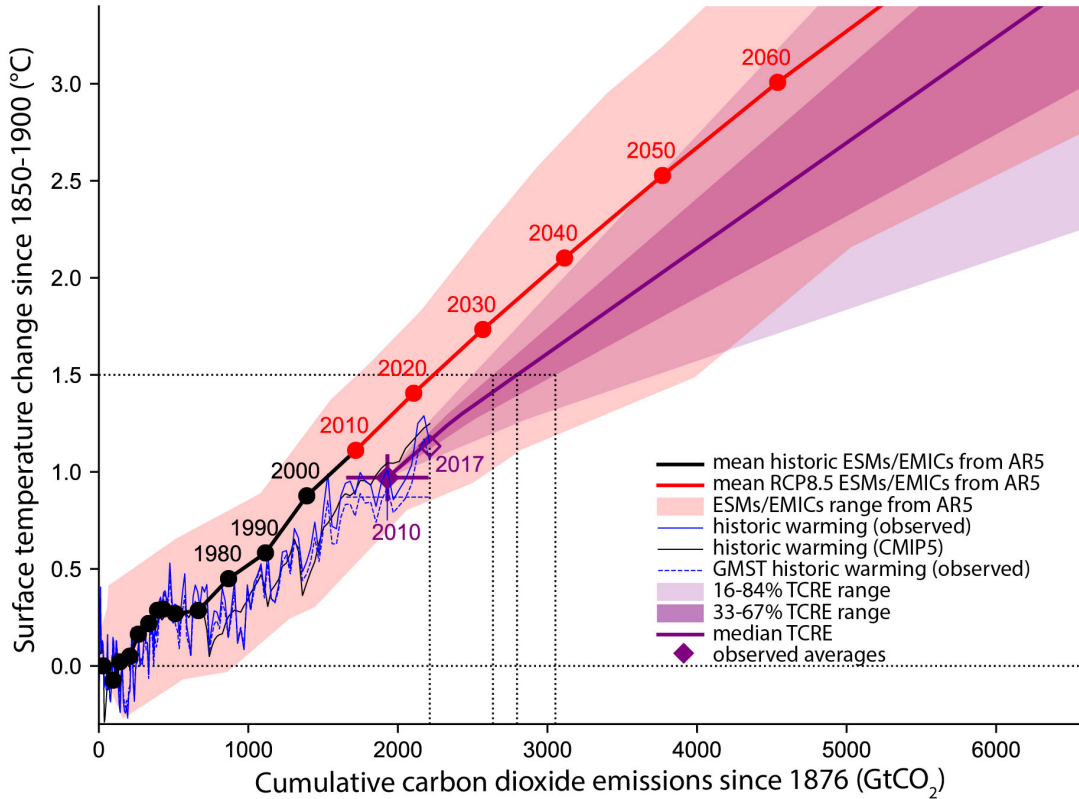
Figure 1-1: Cumulative CO_2 Emissions vs Surface Temperature Change [25]

1.1.1 Climate Factors

As the earth warms, naturally the demand for cooling increases. According to the IPCC, an increase of 1.5C corresponds to an even more pronounced increase in extreme hot days. At 1.5C GSMT warming, the temperature of extreme hot days (heat waves) increases 3C. This figure jumps to 4C at 2C GSMT warming. Additionally, temperature increases are more extreme over land, and may be accompanies by other changes in weather, increasing precipitation in some regions and drought in others. [25]

Climate driven demand for cooling is correlated to the number of cooling degree days (CDDs), which capture the total time and extent to which the ambient temperature exceeds a reference condition. In many populous regions such as Western Europe, household space cooling is uncommon (only 3% in the UK and Germany and 5% in France). However, as climate change slowly turns up our collective global
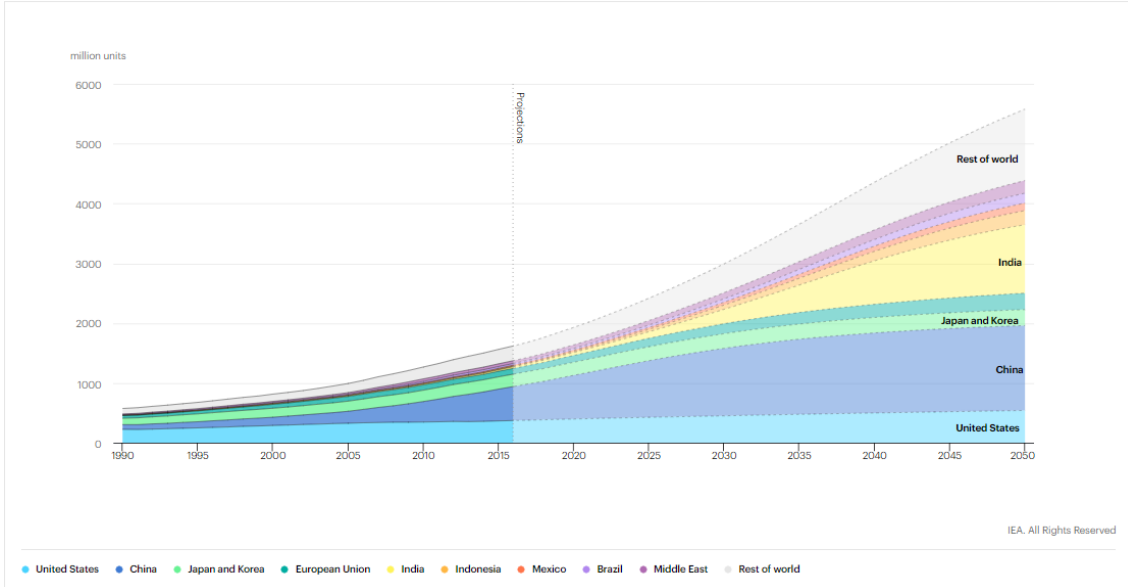
Figure 1-2: Projected global air conditioner stock 1990-2050 (millions)

thermostat, heat waves in these areas increase in frequency. These weather events serve as pain points which drive consumers to invest in AC, leading to a permanent increase in cooling energy demand, even if following Summer temperatures are lower.

The regions with the greatest projected increase in CDDs by 2050 also have the fastest growth rates in population and income. The confluence of these three factors explains the striking increases in demand discussed in this chapter. Climate change is perhaps the most intuitive contributing factor for increasing cooling demand, but it is not the only important driver. [3]

1.1.2   Economic Factors

While climate sets the latent demand for space cooling, economic factors determine to what extent consumers are able to satisfy that demand. While the climates of India and Singapore are similar in terms of CDDs, it is estimated that in Singapore (2018 per-capita GDP = $64,581), 99% of apartments have AC, while in India (2018 per-capita GDP = $2010), only 4% of households have AC. [7][23] While the current market penetration of AC in India is quite low, it is rising rapidly there and in the many other developing countries with hot climates. The clear relationship between

prosperity, climate, and household AC ownership is shown in Figure 1-3. Each data point represents a country, colored by CDD. The high density of red points at the left of the chart indicates the large populations in need of AC but restricted by poverty. Most homes in these hot and poor countries have not yet purchased their first AC, but by 2050 about two-thirds of households worldwide will be AC-equipped. [3]
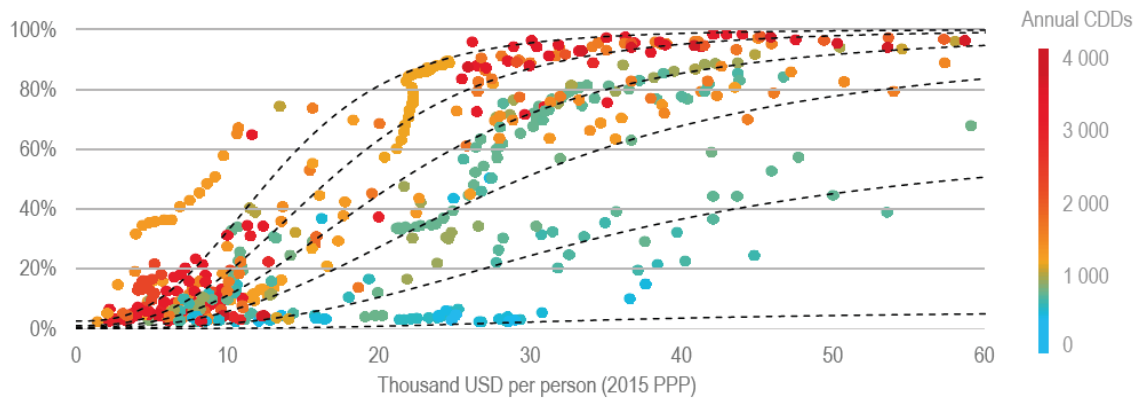
Figure 1-3: Per-capita income vs rate of AC ownership [3]

1.1.3 Demographic Factors

Ignoring all other factors, the world's increasing population alone will drive an increase in cooling demand (and energy demand as a whole). The UN projects an increase in global population from 7.8B in 2020 to 9.7B in 2050. The more complete picture shows several additional factors which bias toward a growing demand for AC. Population growth over in the next 30 years is highest in the hottest parts of the world, largely sub-Saharan Africa. [35] Urbanization also contributes to rising cooling demand. An increasingly urban population means more people working indoors, driving additional demand. Furthermore, the heat island effect drives up ambient temperatures in cities due to a combination of factors, including a significant effect from heat rejection of space cooling systems themselves. The aging population also drives a need for cooling, as older people are generally less heat-tolerant than young. In many cases AC for the elderly is a matter of public health. Hospitalization and mortality rates for the elderly are both known to spike in the wake of heat waves. In the next 30 years, the

percentage of global population over age 60 is projected to increase from 13% to 25% in all regions except Africa. [3]

1.1.4 Implications for Energy Demand

Cooling energy demands put significant strain on the energy grid, especially at peak times. In the Middle East and some parts of the United States, cooling loads represent more than 70% of peak residential electricity demand on the hottest days. [3]

1.2 The State of the Art

1.2.1 Vapor Compression

The vast majority of today's space cooling units are vapor compression systems (VCS) [3]. VCS transfer heat against the natural gradient from a low temperature source to a high temperature sink. The performance of VCS is expressed by the coefficient of performance (COP), see eqn. 1.1.

$$COP_R = \frac{Cooling\ Power}{Work\ Input} = \frac{Q_{cool}}{W_{in}} \qquad (1.1)$$

In its most ideal form, the vapor compression cycle is a reversed Carnot cycle. At the limit, the performance of such a system is given by the Carnot COP, see eqn. 1.2.

$$COP_{Carnot} = \frac{T_{cold}}{T_{hot} - T_{cold}} \qquad (1.2)$$

Where T_{cold} is the temperature of the refrigerant in the evaporator and T_{hot} is the temperature of the refrigerant in the condenser. In industry, two additional terms, energy efficiency ratio (EER) and seasonal energy efficiency ratio (SEER) are commonly used to describe air conditioning performance. EER describes the same metric as COP but is specific to cooling systems (whereas COP can also describe a heat pump in heating mode). EER also implies a specific test condition, which varies by region. In the US EER is tested at an ambient condition of 35C, 50% RH.

Furthermore, in the US, EER by convention uses British thermal units (BTU) for cooling power provided and Watt-hrs (Wh) for work input, requiring a conversion from EER to COP, see eqn. 1.3.

$$EER_{US} = \frac{Cooling\ Power\ (BTU)}{Work\ Input\ (Wh)} = 3.412\ COP \qquad (1.3)$$

SEER gives a more representative estimate of cooling performance over a typical cooling season. SEER is assigned by conducting a series of tests at varying outdoor conditions and calculating a weighted average which represents the cooling season for a particular region. This is useful for consumers as it gives a more accurate performance estimate when purchasing a system. However, since testing standards vary widely by climate, consistent benchmarking is difficult. In this work all benchmark comparisons are made with COP - EER and SEER are only referenced for comparisons between incumbent systems. [3]

The actual refrigeration cycle differs from the reverse Carnot cycle since the turbine is replaced by a throttling valve or capillary tube for practical reasons. This cycle is commonly referred to as direct expansion (DX) refrigeration. The ideal DX cycle consists of 4 processes. [13]

- Isentropic compression in compressor

- Constant pressure heat rejection in condenser

- Constant enthalpy throttling in throttling valve

- Constant pressure heat addition in evaporator

In many mild climates where cooling is needed in summer months and heating is needed in winter months, it is advantageous to run the system in reverse to provide heating. This is accomplished with minimal change to the hardware by including a reversing valve before the compressor. Systems equipped with this function are called heat pumps. Figure 1-4 shows the typical arrangement for a heat pump system operating in cooling mode.
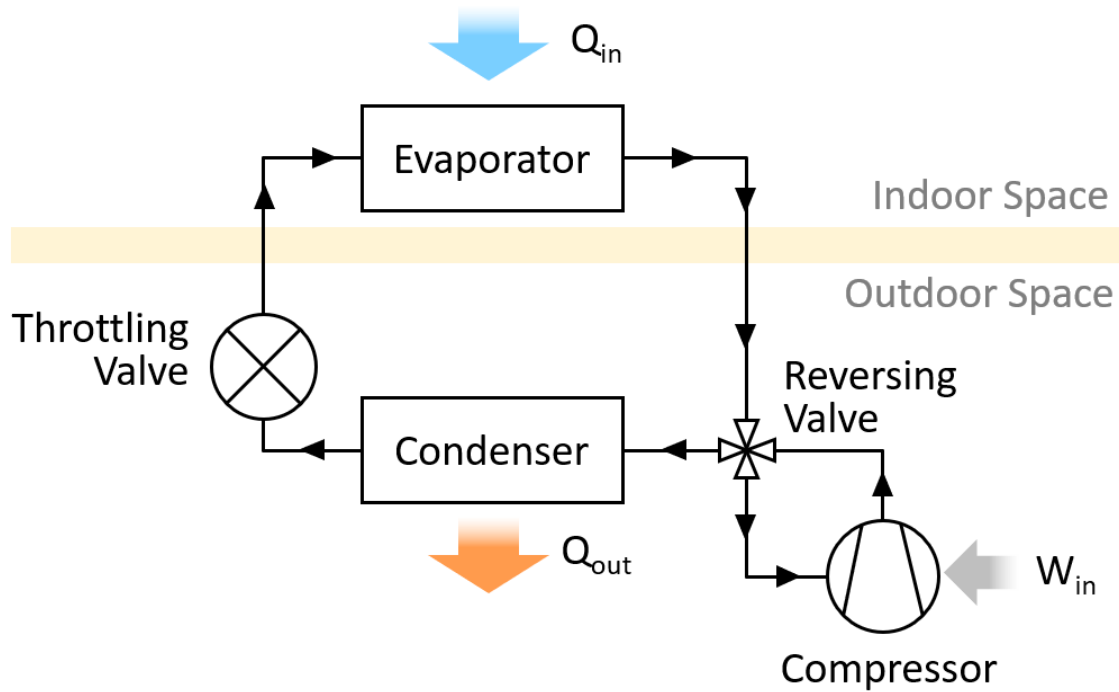
Figure 1-4: Heat Pump in Cooling Configuration

The denominator term in eqn. 1.2 is the temperature difference between the condensing temperature and the evaporating temperature. The performance of the system can be improved by reducing this difference - i.e. lowering condenser temperature or raising evaporator temperature. In order to transfer heat to the ambient environment, the condenser temperature must be above ambient. Similarly, the evaporator temperature must be lower than the indoor space being cooled. The magnitude of this difference is dependent on the effectiveness of heat exchange between the air and refrigerant, so system efficiency may be improved by increasing the size of the condenser or evaporator. This also implies that for a given indoor temperature, when the ambient condition is hotter performance will be lower. To maintain a comfortable condition in the cooled space, both the temperature and humidity of the space must be maintained to certain levels. An indoor condition of 27C and 60% relative humidity (RH) is around the upper limit of human thermal comfort and is used in this work as the standard cooled space condition.

Cooling loads come in the form of sensible loads and latent loads. Sensible loads

Climate	SHR Range
1A-3A. Hot/Humid (e.g. Houston)	0.0-0.9
4A-5A. Hot/Humid/Cold (e.g. Chicago)	0.0-1.0
2B. Hot/Monsoon (e.g. Phoenix)	0.7-1.0
3B-5B. Hot/Dry (e.g. Las Vegas)	0.8-1.0
4C. Marine (e.g. San Francisco)	0.5-1.0

Table 1.1: Typical SHR range for US climate zones

raise the temperature of the indoor space by heat addition, they come from solar irradiance and heat transfer from ambient air (envelope loads), and heat from occupants, lighting, and electronics (internal loads). Latent loads raise the humidity of the indoor space, and come from air changes with the ambient space (if outdoor humidity is high), occupant respiration, cooking, and evaporation from any indoor free water surface. The total load on the building is the sum of all sensible and latent loads. The sensible heat ratio (SHR) is the ratio of sensible load to total load, and varies from 0 (all latent load) to 1 (all sensible load). Table 1.1 shows typical ranges for SHR in several US climates per ASHRAE zone conventions. [28]

Figure 1-5 shows cooling loads and how they are met with present day DX systems. Figure A shows sensible heat ratios from 1.0 - 0.4 from a room condition of 27C and 60% RH. As the fraction of latent load increases, SHR decreases and the load line becomes steeper. Figure B shows the components of latent load and sensible load. To maintain a consistent indoor condition, both loads must be satisfied at the demand SHR. For a system supplying a single stream of air to the conditioned space, this implies the condition of the supplied air must lie along the load line. The mass flow required to meet the load is set by the difference in specific enthalpy between the supply air condition and the room condition, the greater this difference, the less mass flow is required to meet the load. Figure C shows the cooling cycle DX systems must follow to meet latent load. DX systems can only remove moisture by condensing water vapor on the evaporator coils, therefore if any latent load exists the evaporator must run at or below the dew point temperature of the cooled space. As latent load increases, the evaporator temperature must be lowered further until the load line is

reached. At low enough SHR, the load line no longer intersects the saturation line and a conventional DX system cannot meet the load. There are two possible outcomes to this condition. The system may meet the sensible load but fail to meet latent load, causing the cooled space condition to move up vertically on the chart. Alternatively, the system may meet latent load but "overcool" the conditioned space, bringing the indoor condition horizontally to the left on the chart. The former condition results in humidity too high for thermal comfort, leading the occupants to turn down the thermostat and overcool the space, wasting energy. [28]
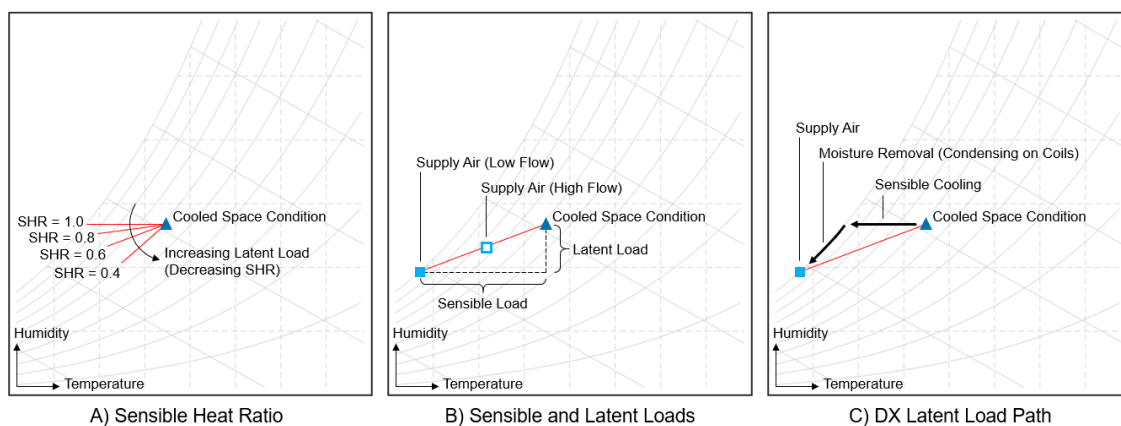
Figure 1-5: Cooling Load Conditions

First law efficiency performance estimates would indicate that DX systems performance falls well short of the ideal Carnot efficiency. For example, at the US EER testing condition, Carnot COP is 37.5, see eqn. 1.4.

$$COP_{Carnot} = \frac{T_{cold}}{T_{hot} - T_{cold}} = \frac{300.15K}{308.15K - 300.15K} = 37.5 \qquad (1.4)$$

However, the IEA reports best in class systems fell between 6 and 12.5 in 2018, less than one-third of ideal performance. More importantly, the market average performance lies between 2.5 and 3.5, depending on country, and is much closer to the lowest available performance (regulated by minimum standards country by country) than the best available [3]. A survey of US Energy Star certified cooling systems over a wide range of capacities gives further insight. [1] The highest COP VC systems in

---

[1]See Appendix A table A.1 for details of surveyed units.

the US are ground-source heat pumps (GSHPs) - see 1.2.2 with COPs up to double the best in class offerings of all other configurations. These systems are aimed at large commercial applications where long-term energy savings justifies their significant up-front cost. However, they are not available at smaller residential scale where most of the energy demand lies [41][3].
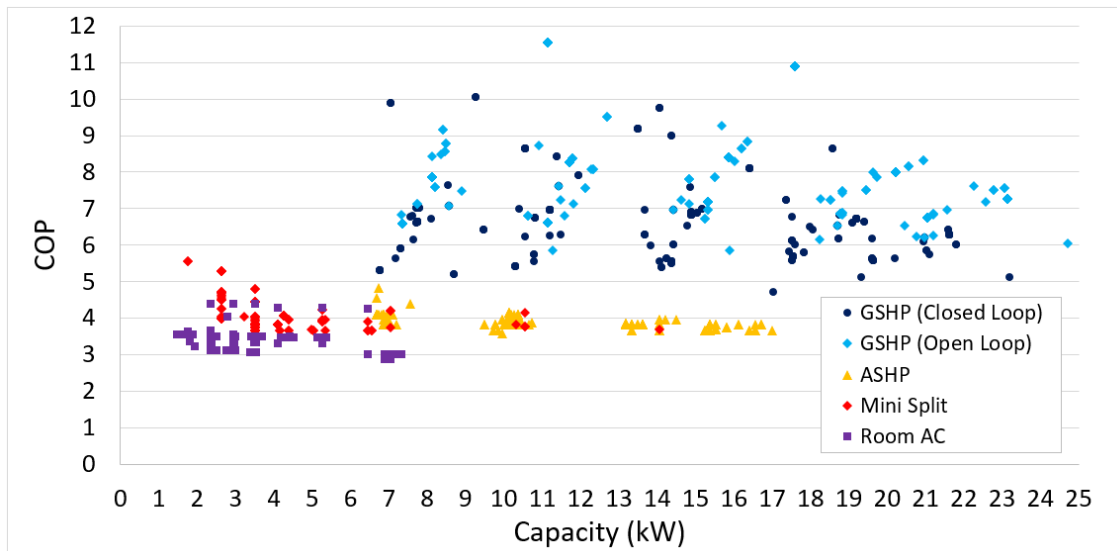
Figure 1-6: Performance of US Energy Star Certified Systems vs Cooling Capacity [41]

The first and most obvious departure from the ideal performance in eqn. 1.4 is that to transfer heat, a gradient must exist between the condensing temperature and ambient, and between the evaporating temperature and indoor temperature. Bilgen and Takahashi [12] compared exergy analysis to experimental data for a room air conditioner with 3.5kW capacity and R410a refrigerant. They include the temperature gradient effects on evaporator and condenser in terms of conductances between source and sink. The study finds exergy efficiencies between 0.35 and 0.22, decreasing with load. The study suggests with optimized design and operation, a performance improvement of 20% is possible. Parasitic powers from fans make up only around 7% of total power at high load condition. Bayrakci and Ozgur [8] perform a similar exergy analysis for several hydrocarbon refrigerants as well as R22 and R134a and find similar exergy efficiencies. Condensing and evaporating temperature are stronger

performance drivers than refrigerant used in the cycle.

Seasonal average energy efficiency ratio (SEER) has slowly risen in recent years, reaching a sales-weighted average of 4.2 in 2016, a 50% improvement from 1990. [3] While performance of DX systems continues to improve, these studies indicate practical limits are within sight and a step-change efficiency improvement is unlikely for these systems.

Beyond the thermodynamic inefficiencies of the vapor compression cycle, there is significant climate impact due to release of refrigerants during operation and at end of life. Global warming potential (GWP) quantifies the carbon cost of refrigerants relative to that of CO_2. More specifically, the GWP relates the radiative forcing in terms of total energy added to the climate system to that of CO_2. Since the persistence in the atmosphere varies from substance to substance, the time horizon must be defined to establish this ratio. The expression of GWP for a given time horizon H is given below in eqn. 1.5 [33]

$$\frac{\int_0^H RF_i(t)dt}{\int_0^H RF_{CO_2}(t)dt} \tag{1.5}$$

Typical time horizons used in literature are 20 years and 100 years. Table 1.2 gives GWP for some common refrigerants used in cooling systems. [33] Chlorofluorocarbons (CFCs) have been phased out under the Montreal Protocol of 1987, with targeted complete discontinuation by 1992 under the Copenhagen Amendment due to their classification as ozone depleting substances (ODS). Under the Montreal Amendment of 1997, HCFCs were also phased out by 2015. The Kigali Amendment of 2016 aims to phase down production and use of HFCs, though the timeline for this reduction extends through the 2040's and is limited to an 85% reduction in use. [18]

Scientists estimate the net effect of the Kigali accord has the potential to reduce atmospheric CO_{2e} by 89.7 GT, which could account for a warming avoidance of around 0.5C. Project Drawdown, a research organization with the goal of finding the most viable climate solutions, ranked refrigerant management as the number 1 solution for

Refrigerant	Type	Lifetime	GWP$_{20}$	GWP$_{100}$
R-12	CFC	100 years	10800	10200
R-11	CFC	45 years	6900	4660
R-22	HCFC	11.9 years	5280	1760
R-134a	HFC	13.4 years	3710	1300
R-32	HFC	5.2 years	2430	677
R-1234yf	HFC	10.5 days	1	<1

Table 1.2: Global warming potential of common refrigerants

reducing climate impact. The effects of the Montreal Protocol and Kigali accord have been studied in China, showing a steep decline in high GWP refrigerant consumption. However, a significant amount of high GWP refrigerants remain "banked" in hardware during its service life. If not properly managed at end of life (EoL), these refrigerants will be released. Based on a sales obsolescence model, the total GWP from scrap refrigerants in China is projected to peak in 2025, with equivalent CO2 from EoL accounting for 1.2% of China's total greenhouse gas emissions. The study highlights the importance of not only making the swift transition to low GWP refrigerants, but also implementing programs for safe collection and destruction of high GWP refrigerants to minimize end of life impacts. [17]

1.2.2   Ground Source Heat Pumps

Ground Source Heat Pumps (GSHPs) are heat pumps with an additional ground loop which allows the system to use the earth as a heat sink for the condenser rather than relying on ambient air. GSHPs consist of three subsystems:

1. ground connected thermal loop

2. heat pump subsystem

3. heat distribution subsystem

The ground connected subsystem consists of a thermal fluid circulated through a series of pipes which allows heat transfer with the ground. The ground loop is often

referred to as the ground heat exchanger (GHE). GSHPs may be divided into two categories - open or closed. Closed systems consist of a GHE with continously circulating fluid (water or antifreeze if needed). Open systems use water drawn directly from an extraction well, and re-inject water to the water table at a different location. Open systems have a slight advantage over closed systems since source water enters the system at ground temperature, rather than shedding heat to the ground through a heat exchange loop. However, open systems are generally less practical and robust. [19][38]

Like other heat pumps, referred to hereafter as air source heat pumps (ASHPs), GSHPs may operate in reverse configuration to provide heat to the conditioned space. Figure 1-7 shows a system diagram of a GSHP operating in cooling mode.
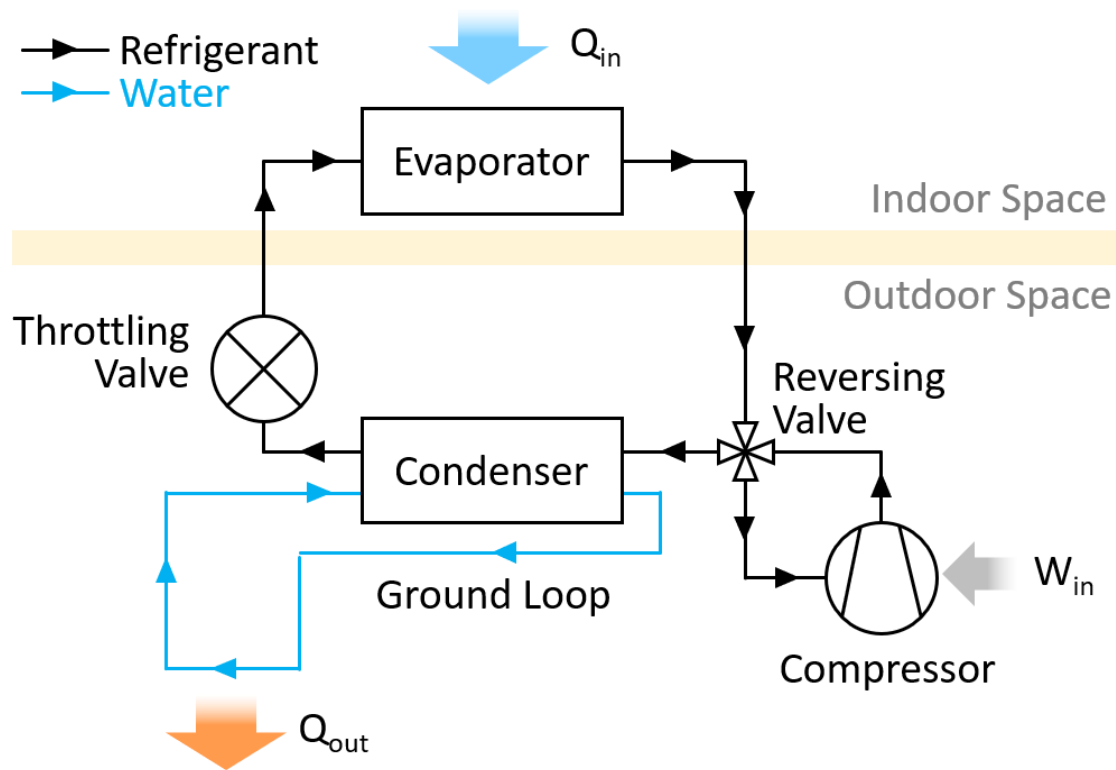
Figure 1-7: Ground Source Heat Pump in Cooling Configuration

GSHPs offer significant COP improvement over ASHPs by reducing the temperature difference between source and sink. This improvement is most pronounced when the difference between ambient air temperature and ground temperature is the great-

28

est. Seasonal and diurnal variation in ground temperature decrease with depth due to the thermal inertia of the soil. For this reason, vertical GHEs consisting of a field of boreholes drilled deep into the earth offer superior performance to horizontal GHEs. In spite of the performance benefits of GSHPs, their substantial installation cost has largely prevented their penetration in the developing world, even in regions with high electricity prices where lifetime savings are greatest. [9]

1.2.3   Evaporative Cooling

Evaporative cooling is a promising low energy alternative to vapor compression cooling systems. Unlike VCS, evaporative cooling is not bounded by Carnot efficiency since the refrigerant (water) delivers its cooling effect directly and operates in an open cycle rather than a closed cycle. Under the right climate conditions, evaporative cooling can reduce energy consumption by as much as 70% relative to conventional VCS. [37] The simplest form of evaporative cooling is direct evaporative cooling (DEC), in which water is evaporated directly into the airstream used for cooling the conditioned space (known as the process airstream). In the most common form, water drips slowly onto a wetted media and spreads by "wicking" on the surface and capillary action through the media. Air flows through the wetted corrugated channels, cooling it as water evaporates. The process is adiabatic, so all sensible heat lost by the air is gained as latent heat. This implies the upper limit for sensible cooling in a DEC is the wet bulb temperature. DEC performance is measured by wet bulb effectiveness - eqn. 1.6.

$$\eta_{wb} = \frac{t_{in} - t_{out}}{t_{in} - t_{wb}} \tag{1.6}$$

In recent years, many empirical [40], numerical [11], and experimental [32][43] studies have been conducted to characterize performance of DECs, finding effectiveness up to 95% is feasible. The primary benefits of DEC are simplicity and efficiency, since there is only a single airstream, the only electrical power demand is a single fan and low-flow water pump. In dry regions where wet bulb temperatures are low, DEC

is an attractive option. In many humid climates however, DECs cannot satisfy thermal comfort for both temperature and humidity. Furthermore, the evaporative pad presents hygienic concerns if not maintained properly. Indirect evaporative cooling (IEC) systems use a second airstream, called the working air, to evaporate into, then transfer heat from the process air to the working air through sensible exchange without humidifying the process air. Unfortunately, the wet bulb effectiveness of these systems suffers due to the additional heat exchange step, and is generally limited to 40-60%. [37]

Dew point evaporative cooling, also known as M-cycle cooling after its inventor Valeriy Maisotsenk, is similar to IEC but instead of the working stream being supplied by ambient air, air from the dry channel is diverted to the wet channel after first being sensibly cooled in the dry channel. Only a fraction of the process stream air is cooled, but the air may be cooled below its wet bulb temperature, theoretically down to the dew point. Dew point evaporative cooling can reach dew point effectiveness (defined the same as eqn. 1.6, but with T_{wb} replaced by T_{dp}) between 0.6-0.85 depending on inlet conditions. [37] As with DEC and IEC, dew point cooling has the greatest capacity in dry climates.
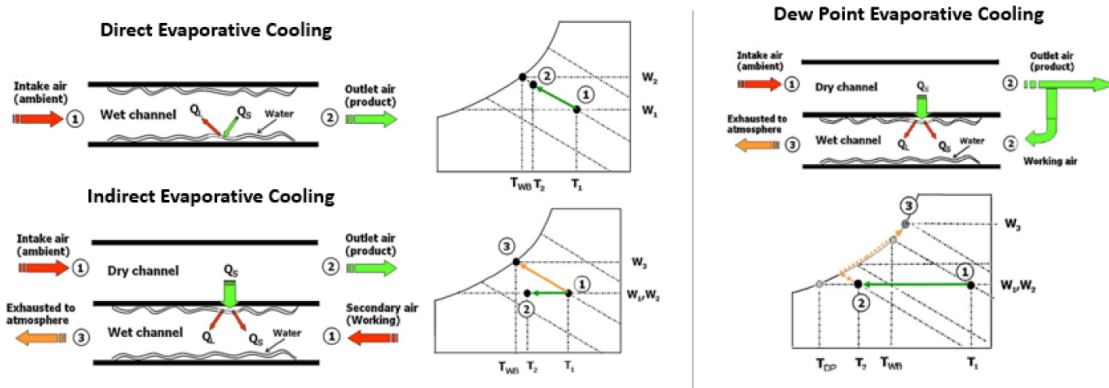
Figure 1-8: Flow and process diagrams for DEC, IEC, and dew point cooling

1.2.4 Desiccant Dehumidification

As discussed in 1.2.1, modern vapor compression technology is inefficient at meeting latent loads in air conditioning. Desiccant dehumidification is an alternative approach

to remove moisture from air. Desiccant dehumidification comes in two forms - solid desiccant systems and liquid desiccant systems. This method relies on substances with low vapor pressure at their surface to pull moisture from the air by adsorption (solid desiccant) or absorption (liquid desiccant). A cycle is required to regenerate the desiccant once it is saturated, enabling continuous drying. The steps are as follows.

1. Sorption - desiccant begins dry and cool, its low vapor pressure draws moisture from the air, sorption may continue until the surface vapor pressure equals that of the air it is exposed to.

2. Desorption - the desiccant is heated and placed in a separate airstream. The heating increases its surface vapor pressure allowing moisture to be drawn out by the regeneration stream

3. Cooling - after moisture has been released and the desiccant is dry, it must be cooled to return it to a state of low vapor pressure so the cycle can continue.

Numerous configurations of dehumidifcation systems exist for both liquid and solid desiccant types. Figure 1-9 shows four types commonly used. Solid desiccant systems include the desiccant wheel (top left) and packed bed (bottom left) type. In a desiccant wheel, the solid desiccant is embedded in a honeycomb, forming channels parallel to the axis of rotation. The wheel rotates between a process and regeneration air-stream. This type has the advantage of high surface area and low pressure drop, but does not lend itself well to compact systems. The packed bed style consists of two "towers" with loose beads of desiccant. Air is alternated between the two beds by switching valves at the inlet and exit. Liquid desiccant systems include spray towers (top right) and liquid air membrane energy exchanger (LAMEE) systems (bottom right). In both systems the liquid desiccant is pumped between process and regeneration stages, the difference is in how the moisture exchange occurs. In spray tower systems, the liquid desiccant is sprayed through nozzles near the top of the vessel forming a mist. As the mist falls, air flows up against the direction of flow, allowing absorption or desorbtion to occur. This method has the advantage of favorable mass

transfer characteristics due to high surface area, but may allow entrainment of the desiccant into the air-stream. [24] LAMEE systems use membranes with microscopic pores which allow water to pass but prevent carryover of the desiccant. LAMEEs come in forms similar to conventional heat exchangers: shell-and-tube and flat plate. The shell-and-tube style consist of a bundle of hollow fibres in a shell. These offer impressive surface area to volume ratios as high as 2000 m^2/m^3. Flat plate style LAMEEs are also common, and consist of alternating layers of air and fluid passages. These can be configured in parallel, crossflow, or counterflow orientation [45].
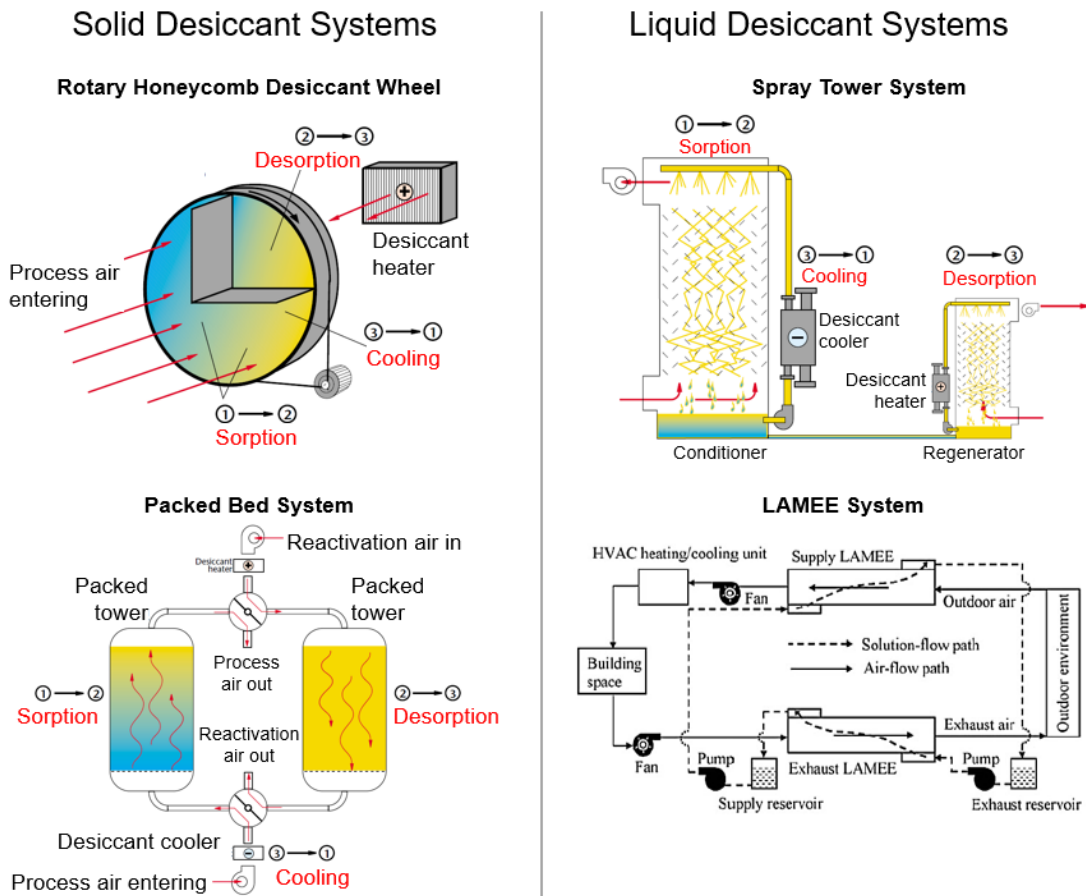
Figure 1-9: Solid and Liquid Desiccant Dehumidification Systems
[24] [45]

1.2.5 LAMEEs

LAMEE performance, configuration, and design is an active area of research and much progress has been made in recent years to move these devices toward widespread use. Bai [6] constructed a LAMEE and studied its experimental performance using $CaCl_2$ liquid desiccant. The effects of solution concentration, mass flow ratio, NTUs of the exchanger, and inlet temperature were considered. Max total effectiveness was found to be 0.53, and improved with lower inlet solution temperature. Li [30] conducted a numerical study of a dehumidifier with LAMEE exchangers, looking at many of the same parameters and optimizing for overall system effectiveness. They found NTU and mass flow rate ratio (m^*) to be the most important driving parameters, and that effectiveness does not improve substantially beyond NTU = 2 and $m^* = 4$.

Wang [42] quantified the thermodynamics of the ideal liquid desiccant dehumidification cycle and explored the implications for efficiency limits at different operating conditions through energy and exergy analysis. A similar method is used for the regeneration energy calculations for the ideal cycle studies in Chapter 2. A run-around membrane energy exchanger RAMEE consists of two LAMEEs used together as an enthalpy recovery device. RAMEEs provide no cooling of their own but assist an existing HVAC system by recovering energy of make-up air. Kassai [27] numerically investigated the performance of a run-around membrane energy exchanger (RAMEE) and found up to 95% total effectiveness is possible, and an ideal Cr^* of 3.2 for optimal system performance where Cr^* is liquid desiccant capacitance over air capacitance.

1.2.6 Liquid Desiccant Cooling

Liquid desiccant dehumidification and evaporative cooling may be combined to create a liquid desiccant air-conditioning system (LDAS). LDAS has significant energy-saving potential since the cycle is primarily heat-driven in contrast to the work-driven vapor compression cycle. Desiccant dehumidification enables effective evaporative cooling in climates that would otherwise be too humid for it, and boosts the capacity of evaporative cooling alone. Kumar [29] investigates desiccant selection for an LDAC

system, considering LiCl, CaCl$_2$, LiBr, and KCOOH in a simple liquid desiccant cooling circuit with storage. LiBr was preferred in spite of 30% higher initial cost than LiCl due to its lower operating costs. Xiong [44] developed a novel two-stage liquid desiccant dehumidification system using LiCl and CaCl$_2$ to assist the dehumidification. This system reduces exergy loss in heat recovery and reduces the irreversibility of the process by pre-dehumidifiying with CaCl$_2$. The study found nearly three-fold thermal COP improvement from 0.24 to 0.73 and energy storage density of 237.8 and 395 MJ/m^3 for CaCl$_2$ and LiCl respectively. Cheng [14] explored the possibility of an electrodialysis regenerator to enable regeneration of the liquid desiccant even in hot and humid environments. They found ideal performance of such a system gives a COP over 7 when conductivity of the liquid desiccant is high. Kozubal [28] developed and patented a novel desiccant enhanced evaporative air conditioner (DEVap), which combines dew point evaporative cooling and liquid desiccant dehumidification. DEVap combines dehumidification and cooling into a single core which gives the advantage of close thermal coupling between dehumidification (which requires a heat sink) and evaporative cooling (which requires a dry air source). The DEVap system claims 30-90% energy savings over conventional VCS technology without the use of harmful refrigerants. Figure 1-10 shows the physical core geometry of the DEVap system.
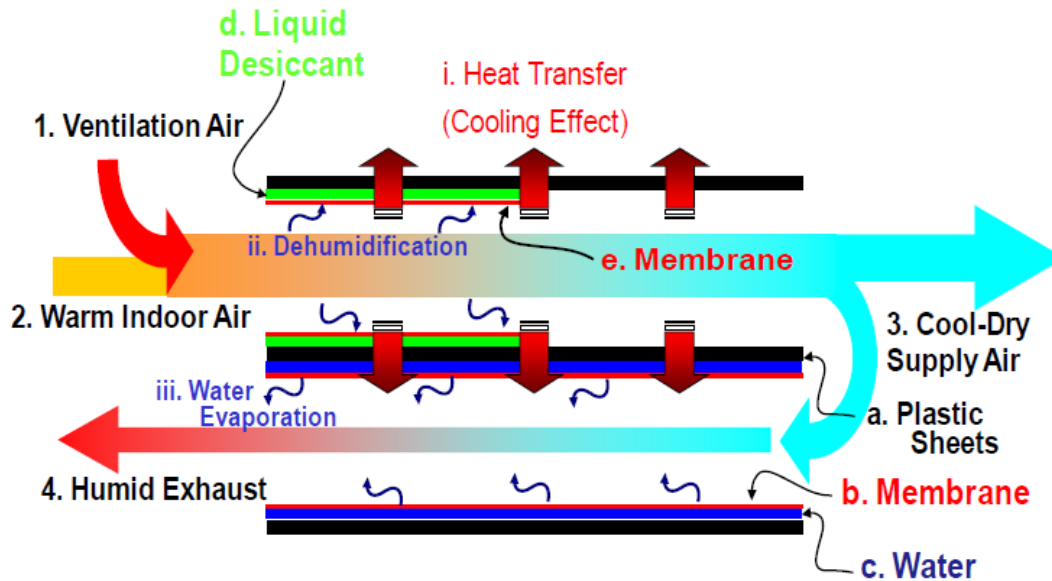
Figure 1-10: DEVap Cooling Core

[28]

In many ways the DECAL system is similar to DEVap, but does not have direct thermal exchange between dehumidification surfaces and evaporative surfaces and uses direct evaporative cooling rather than dew point cooling - see section 2.3 for details.

Abdel-Salam [1] conducted a thermo-economic study of an LDAC system with solar regeneration in eight configurations varying the heating source and use of an energy recovery ventilator (ERV). They found the best system in terms of life cycle cost uses a solar thermal collector as the primary heat source, with natural gas as a backup and without an ERV. Life cycle cost was always lower when a solar thermal collector was included.

Chapter 2

System Design

The direct evaporative closed air loop (DECAL) system is a novel liquid desiccant cooling cycle designed to provide high efficiency residential cooling to meet rising demand. This chapter lays out the requirements for the system, walks through the thermodynamic cycle, and identifies the ideal performance limits of such a system relative to those in similar LDACs.

2.1 Figures of Merit and Design Constraints

The following conditions must be met to maximize the climate impact of a next generation high efficiency air conditioning system.

1. Reduced carbon footprint through improved efficiency

2. Widespread adoption in the marketplace

Cooling energy demand growth in the next 30 years will come primarily in residential cooling [3]. The number of room air conditioners in use globally is expected to grow from around 1.2B today to 4.5B by 2050 [36]. Therefore the most impactful solution should fit in the residential size class - between 2 and 7 kW of cooling provided. As shown in figure 1-6, the most efficient units available today in this range are mini-split systems with COP under 6. IEA studies [3] show mini-split systems

dominate the current and future residential global market, for this reason mini-splits are used as the benchmark incumbent system for this study.

Although LDAC systems show promise for substantial energy savings [28][44][31], none have yet been commercialized at large scale. The novel cycle proposed in this work seeks to overcome this obstacle by maintaining a balanced focus on both form and function to deliver a solution poised for widespread adoption. To this end, it is imperative to address building integration and consider the success of ductless mini split systems.

Split systems have the benefit of installation flexibility since only refrigerant lines connect the modules and the cooling modules deliver air directly to the conditioned space, eliminating the need for air ducts. This greatly simplifies installation and enables retrofitting into existing building stock without major renovation. Many modern split systems even offer "DIY" installation with pre-purged lines which require no specialized tools. This configuration also eliminates the parasitic loss of air drag in ducting, reducing fan power requirements and improving efficiency. As the name implies, split systems consist of multiple modules - typically an outdoor unit which includes the compressor and condenser, and one or multiple indoor evaporator units. This configuration further simplifies installation by splitting up the mass and volume of the device. While mini splits enjoy these practical advantages, they suffer the limitation that no air is exchanged between outdoor and indoor units. This limits their use in buildings with large make-up air requirements such as hospitals, office buildings, and shopping centers. In residential spaces there is enough natural infiltration from inhabitants ingress and egress and leakage to give adequate ventilation. In fact, limiting exchange provides an advantage since ventilation accounts for over half of all thermal losses in modern buildings [27]. As discussed in 1.2.1, the method of moisture removal in VC systems significantly reduces their efficiency, and desiccant based systems are well suited to handle moisture. This work seeks to answer the question: *Can we design a liquid desiccant based air conditioner with the form factor advantages of a mini split system?*

Table 2.1 summarizes the standard sizing conditions used in this study. The

system is optimized to this design point.

Condition	Value	Units
Indoor dry bulb temperature	27	C
Indoor relative humidity	60	%
Outdoor dry bulb temperature	35	C
Outdoor relative humidity	60	%
Cooling load	7	kW
Sensible heat ratio	0.75	W/W

Table 2.1: Sizing Conditions Used In This Study

2.1.1 Physical Envelope

A survey of physical dimensions for Energy Star rated mini split units from [41] shows total system volume (indoor + outdoor unit) per Watt of cooling power. [1] For a high-efficiency system to be competitive it should be of similar size to current offerings, but with some allowance to acknowledge the efficiency benefits over incumbent systems. Therefore a target of 150 cm^3/W is set. Furthermore, to facilitate transportation and maintain conventional building integration, the maximum dimension for all modules (except the solar thermal collector if used) is limited to 1m at the 7kW design point.

2.1.2 Thermal Coefficient of Performance

Unlike VC systems where most of the energy supplied is electrical power to the compressor, LDAC systems are thermally driven. Regeneration heat is required to concentrate the desiccant after it absorbs moisture from the air. The thermal coefficient of performance is defined by equation 2.1 below.

$$COP_{th} = \frac{Cooling\ Output\ (W)}{Heat\ Input\ (W)} \tag{2.1}$$

---

[1]See Appendix A table A.1 for details of surveyed units.
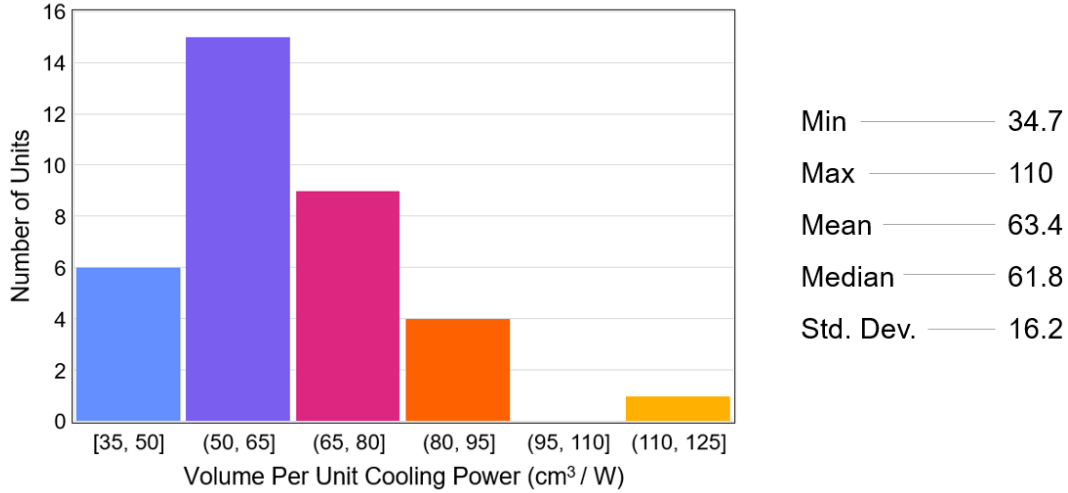
Figure 2-1: Energy Star Split Systems Specific Volume

Regeneration heat can come from waste heat, solar thermal energy, or a heat pump. If solar energy is used, the size of the collector required depends on the thermal COP of the system, the relationship between incident solar irradiance and cooling load, and the storage capacity of the system. Detailed design of the solar thermal collector requires a more specific application which is beyond the scope of this study, but to keep collector size small the target COP_{th} is set to 0.70. This target is reasonable based on a survey of solar assisted desiccant evaporative cooling systems by Jani [26] in which COP_{th} ranged from 0.25 to 1.38. [2]

2.1.3   Electrical Coefficient of Performance

Electrical COP of the system is defined by equation 2.2 below.

$$COP_{elec} = \frac{Cooling\ Output\ (W)}{Electrical\ Input\ (W)} \tag{2.2}$$

As discussed in 1.2.1, COP for evaporatively cooled systems is not bounded by Carnot limits. Without the burden of a mechanical compressor, electrical COP can be quite high since the only power draw comes from fans, pumps and electronics.

---

[2]This study was a survey of solid desiccant systems rather than liquid, but the thermodynamic performance of such systems is similar to LDAC

Coolerado [16] cites an electrical COP over 18 for the M50C series dew point evaporative coolers. The global cooling prize [36] proposed an 80% reduction in energy consumption from a present day baseline COP of 3.5 is needed to offset the dramatic increase in demand coming in the next 30 years. A target electrical COP of 20 is used in this study.

2.1.4 Cooling Unit Airflow

The airflow required by the indoor cooling unit to meet a given sensible demand depends on the room temperature, the temperature of the cold air provided, and the density of the air. Indoor temperature is specified by the user and is therefore a function of human thermal comfort. Thermal comfort is dependent on dry bulb temperature and humidity, and AC cooling capacity is generally measured with indoor conditions near the upper limit of comfort. In the US, SEER testing calls for an indoor condition of 26.7C & 50.7% RH. For this study, an indoor condition of 27C and 60% RH is used. Furthermore, the sensible heat ratio is set at 0.75 unless specified otherwise. The sensible cooling is given by equation 2.3.

$$Q_{sens} = Q_{tot}SHR = \dot{v}\rho c_p \left(T_{room} - T_{cool}\right) \qquad (2.3)$$

Where $\dot{v}$ is the volume flow rate of air (m^3/s), ρ is the density of air (kg/m^3), c_p is the specific heat of air, T_{room} is the temperature of the conditioned space, and T_{cool} is the temperature of the cooling air provided by the indoor unit. For practical purposes such as noise, it is necessary to limit the volume flow of the indoor unit. A typical mini split system indoor unit flows around 3 $m^3/min/kW$ so the cool air temperature of the cycle must be low enough to meet that flow - substituting into equation 2.3 and solving for T_{cool} the required outlet temperature is 14.4C. Ideal cycle studies show this target temperature is infeasible for the target condition. Commercially available evaporative coolers do typically require more airflow due to the smaller temperature difference between outlet condition and room condition. The target specific flow is set at 6 $m^3/min/kW$ of cooling.

Table 2.2 summarizes the figures of merit used in this study.

Figure of Merit	Target	Units
System COP$_{elec}$	20	W/W
System COP$_{th}$	0.70	W/W
Specific Volume	150	cm^3/W
Indoor Unit Flow Rate	6	m^3/min/kW

Table 2.2: Figure of Merit Targets

2.2   System Overview

The DECAL system consists of four modules, the process module, DEC module, regeneration module, and cooling module. Each module serves an essential function to achieve the net effect of heat and moisture removal from the conditioned space. The modules are discrete in their function and may be co-located or physically separated as needed based on the physical limitations of the installation. Figure 2-2 shows a simplified block diagram of the system.
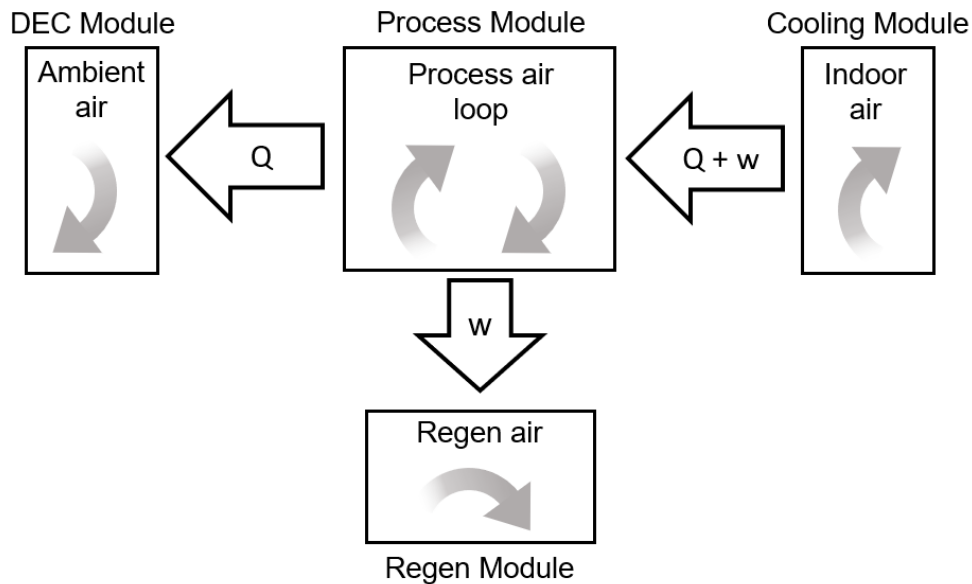

Figure 2-2: DECAL Simplified System Diagram

The DEC and regeneration modules reject heat and moisture to ambient air, and the cooling module captures heat and moisture with the indoor air. Liquid desiccant (LD) is pumped between modules and serves as the heat and mass transfer fluid for the system. A water supply from a water reservoir or municipal source is required for the DEC and process modules. Each module requires electrical power as well to run pumps and fans. However, there is no direct air exchange between modules, or between the indoor space and ambient air. In this way, the system is most similar to a distributed system like a chiller, in which a water or antifreeze solution circulates between the cooled space and a remote cooling system. Ductless mini-split systems offer similar flexibility, with refrigerant lines running between indoor evaporator units and an outdoor unit containing the compressor and condenser coil. In each case, the advantage is in having compact lines connecting modules, rather than large air ducts. Smaller lines are easier to retrofit into existing buildings, giving a practical advantage. There is also a cycle benefit to such systems, since parasitic heat gain on the lines is proportional to surface area, and line sizes may be dramatically smaller for systems circulating water, refrigerant, or liquid desiccant. Unlike the chiller or mini-split system, the DECAL system enables moisture removal through the circulated liquid desiccant. This allows the system to meet latent loads much more efficiently, avoiding the drawbacks discussed in section 1.2.1. There is no vapor compression cooling in the DECAL system - all cooling is provided by evaporation of water. There are two direct evaporative coolers (DECs) which operate on different air-streams to produce cooling. The system is designed to allow the DECs to produce an additive temperature effect. The first DEC acts on ambient air and is thus limited to the ambient wet bulb temperature. The second DEC acts on the closed air-stream which is cooler and drier than the ambient condition. This allows the system to reach temperatures below the ambient dew point, which is the limit for conventional evaporative cooling systems.

The DECAL system includes two liquid desiccant loops, the cooling loop and the process loop. Both loops use a common liquid desiccant - either LiCl or $CaCl_2$ (both are considered in this study). The LD process loop operates at high concentration and serves primarily to dry the process air-stream. The LD cooling loop operates

at mild salt concentration and provides both the sensible and latent cooling to the conditioned space. The two LD loops operate independently except for a mixing valve after the indoor cooling LAMEE in the LDC loop and after the process LAMEE in the LDP loop which allows the cooling loop to regenerate by trading a small volume of dilute solution with equal volume of strong solution from the process loop. In this way, only a single regeneration circuit is needed for both LD loops - see figure 2-3 for the full system diagram. The lower concentration of the LD cooling loop allows it to operate at cooler temperatures without risk of crystallization. It is also favorable to use a lower concentration in the cooling circuit to avoid over-drying the conditioned space. By metering the exchange between LDC and LDP loops, the concentration of the LDC stream may be controlled to give independent control of sensible and latent cooling and match the SHR of the conditioned space.

2.3 Cooling Cycle

The DECAL system provides all cooling power through direct evaporative cooling. As discussed in section 1.2.3, the lower limit of outlet air temperature in a DEC is the wet bulb temperature of the inlet air stream. In many climates, particularly in the tropics where future demand is greatest, the ambient wet bulb temperature is still above human comfort and thus DEC alone is inadequate. However, when combined with desiccant dehumidification, a staged evaporative cooling system may overcome this obstacle. In simplest form, a 2-stage direct liquid desiccant evaporative cycle would consist of three steps.

1. Stage 1 DEC from ambient

2. Desiccant dehumidification in a LAMEE

3. Stage 2 DEC from the dry condition

Here we assume both evaporative processes are constant enthalpy, and that the stage 1 DEC cools not only the process air stream, but also the liquid desiccant used

44
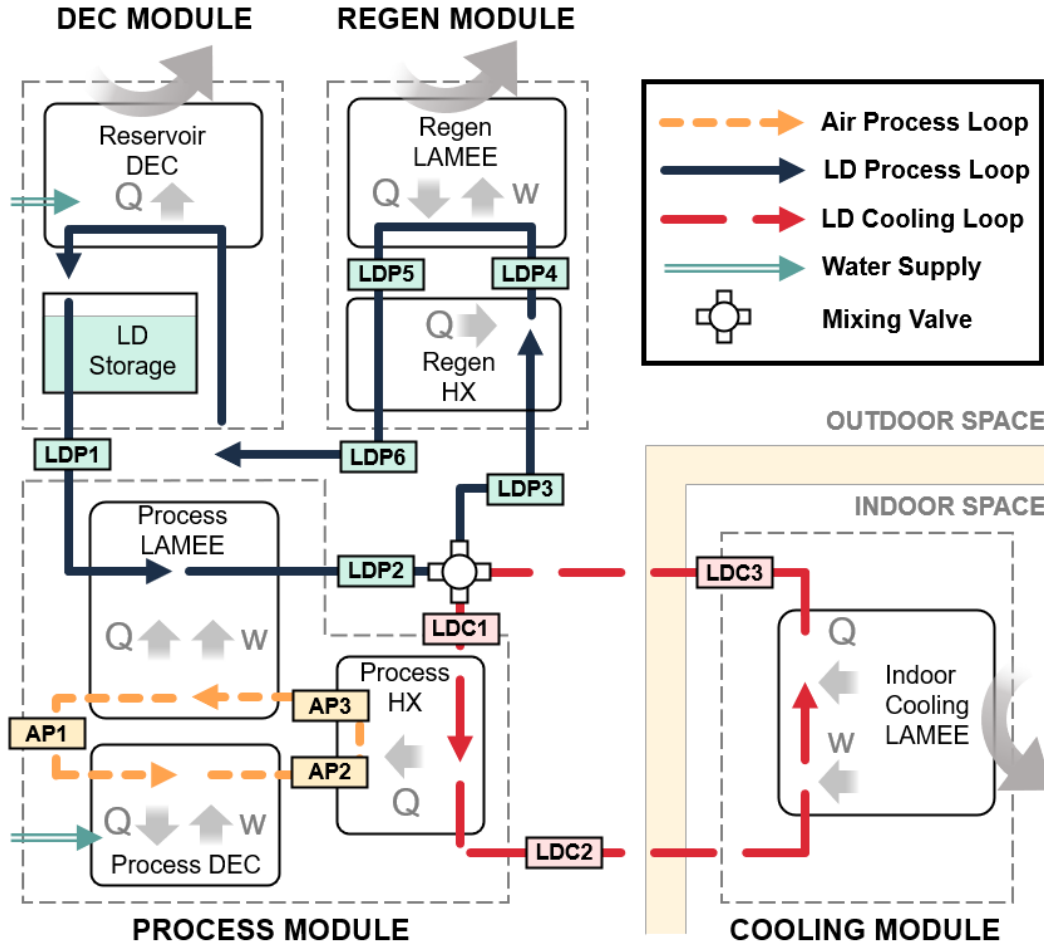
Figure 2-3: Full System Schematic

for dehumidification. In an ideal counterflow LAMEE, most of the heat of adsorption goes to the liquid desiccant stream [22], so process 2 is isothermal. The overall cooling effect depends on the ambient wet bulb, which sets the cooling capacity of stage 1, and the liquid desiccant equilibrium vapor pressure (a function of mass concentration and temperature, see 3.5.2), which sets the capacity of stage 2. At the limit, the maximum achievable capacity of stage 2 is set by the saturation limit of the liquid desiccant used in the cycle. Figure 2-4 shows an ideal two stage evaporative cooling cycle using $CaCl_2$ from an ambient condition of 35C & 60% RH. At this climate condition even an ideal DEC cannot provide cooling in a single stage since ambient T_{wb} is above the room temperature. However, with a 2-stage system an outlet condition of 17C is possible.

In a direct 2-stage system, a single air stream supplies cooling directly from the ambient condition. Wang [42] showed the ideal regeneration energy is proportional to the net water vapor absorbed by the system. So in a direct 2-stage system, the regeneration heat scales with the difference between the ambient wet bulb humidity and the saturation limit humidity at reservoir temperature. The thermodynamic advantage of the DECAL cycle comes from the use of recirculated air in a closed loop rather than ambient air. This allows the system to recover much of the dehumidification energy which would otherwise be lost in a direct supply system. The DECAL system only needs to regenerate the moisture gain from the stage 2 DEC, while a direct system needs to regenerate moisture gain from both stages, as well as the difference between the supply air condition and the ambient condition humidity.

Figure 2-4: DECAL Staged Evaporative Cooling

In this way the DECAL system is able to provide sensible cooling well below the ambient dew point by evaporative means alone, and minimize the regeneration
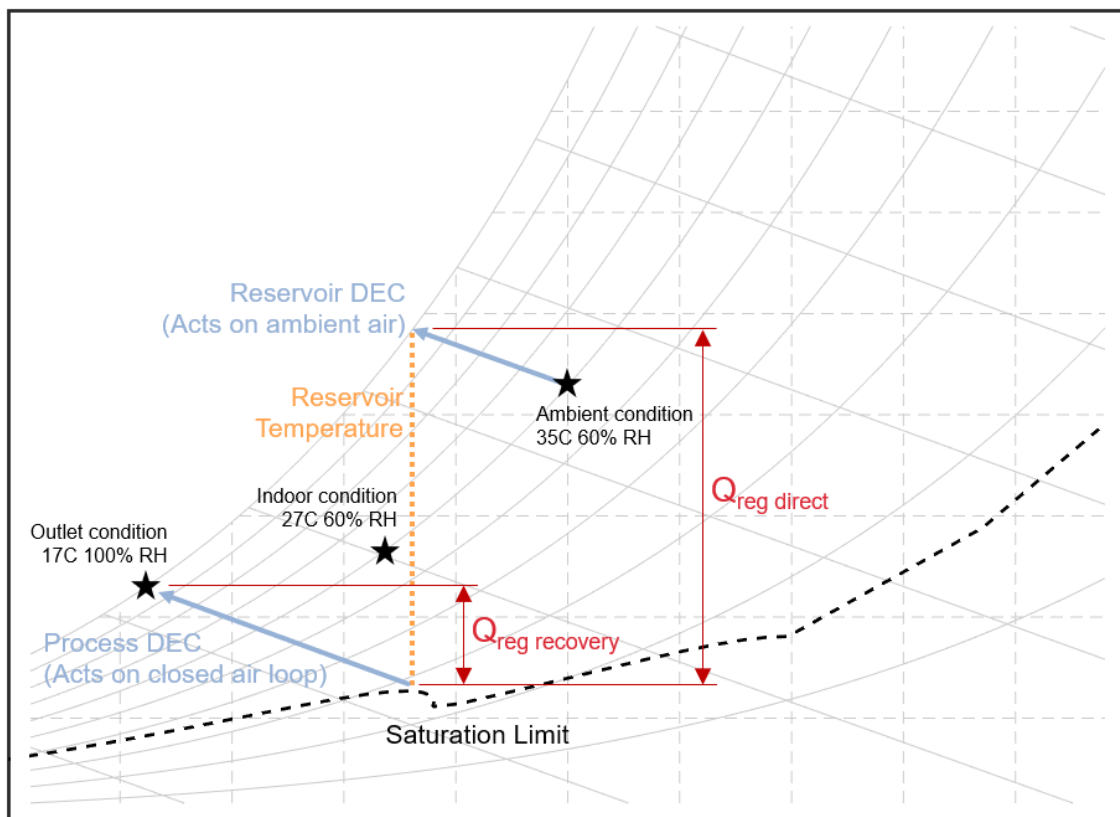
energy required for continuous operation. DECAL uses direct evaporative coolers rather than more sophisticated evaporative cooling systems such as indirect-direct or dew point cooling. The rationale for this choice is driven by two factors. Dew point coolers require a second working air stream with similar mass flow to the process stream. This requirement is incompatible with the closed air loop since all air in the loop must be recycled, so the working stream would need to be pulled from ambient, increasing the regeneration heat required. A dew point cooler could be used in place of the reservoir DEC, however volume constraints make this inadvisable. Both dew point and indirect-direct coolers transfer heat between two air streams. Air-to-air heat transfer requires large surface areas to be effective, and would make the system less competitive on specific volume.

2.4   Air Process Loop

The closed air loop is the heart of the DECAL system. Air flows between three exchangers in the process module to provide sensible cooling to the liquid desiccant cooling loop. The cycle begins at the inlet to the process DEC just after exiting the process LAMEE (AP1). At this condition the air has been dried well below ambient humidity (around 20% RH at the design condition). Air enters the direct evaporative cooler and is sensibly cooled to near its wet bulb temperature (AP2). This is the coldest point in the cycle and must be well below the room condition for the cycle to be viable. The cold air then enters the process HX where it picks up heat from the LDC stream and warms back up near (but below) the room temperature (AP3). At this point the air returns to the process LAMEE where it transfers the moisture gained in the DEC to the LDP stream and begins the cycle again. Depending on the relationship between ambient wet bulb temperature and room condition, AP3 may be slightly warmer or cooler than AP1. Figure 2-5 shows the relevant sections of the cycle on the psychrometric chart and on the system diagram.
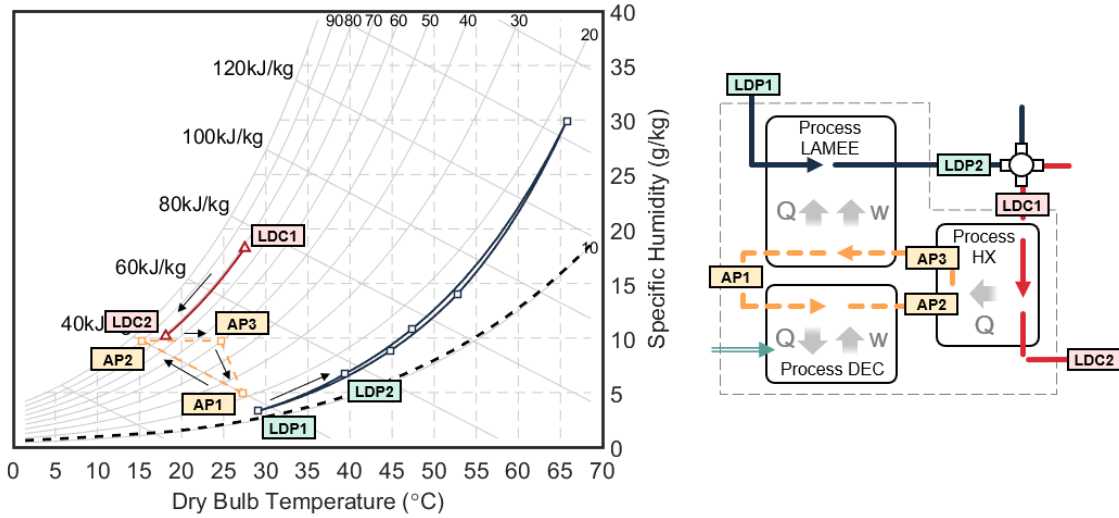
Figure 2-5: Air Process Loop Cycle and Diagram

2.5 LD Cooling Loop

The LD cooling circuit provides sensible and latent cooling to the indoor space. It is the DECAL equivalent of the evaporator in a conventional VC system. Liquid desiccant flows between the indoor and outdoor space through small pipes (less than 1" diameter). The process begins at the process heat exchanger inlet (LDC1) where sensible heat from the cooled space is transferred to the process air stream, cooling the LD stream without changing its mass concentration (LDC2). After cooling, the LD enters the indoor cooling LAMEE, where it takes both heat and moisture from the cooled space, heating it and reducing its mass concentration of liquid desiccant (LDC3). The LDC stream is heated beyond the sensible heat transferred from the cooling air due to the heat of absorption from the latent transfer. The LD then enters the mixing valve where a small volume (less than 5% of total flow) is transferred between streams. Since the LDP stream always operates at higher mass concentration than the LDC stream, this regenerates the LDC stream and dilutes the LDP stream. A small amount of heat is generated when the stronger LDP stream flow mixes with the LDC stream flow (enthalpy of dilution) however, since the total mass transferred is small relative to the total flow, this effect is negligible. Figure 2-6 shows the relevant sections of the cycle on the psychrometric chart and on the system diagram.
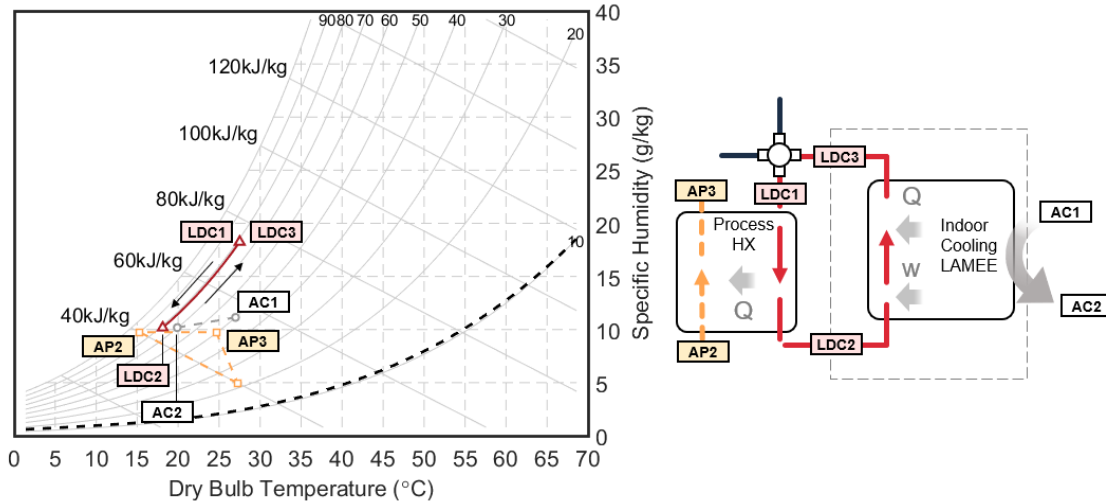
Figure 2-6: LD Cooling Loop Cycle and Diagram

2.6   LD Process Loop

The LD process loop carries the moisture from the process DEC and latent load removed from the conditioned space to the regeneration LAMEE where it is released outside, allowing the system to operate continuously. The process begins with liquid desiccant exiting the LD storage tank where it has been cooled by the reservoir DEC near the ambient wet bulb temperature (LDP1). At this point the LD is concentrated and at the lowest temperature in the cycle, so its margin to the solubility limit is smallest. The design point condition for solubility margin is set to 5%, so the mass concentration at this point is 95% the concentration at which it would begin to precipitate from solution. For $CaCl_2$ this is around 0.47 g/g and for LiCl this is around 0.44 g/g. The LD enters the process LAMEE where it dries the process air, diluting the solution and heating due to heat of absorption (LDP2). The LDP stream is then diluted by mixing with the LDC stream at the mixing valve (LDP3). It then enters the cold side of the regen heat exchanger, or economizer, which recovers some of the heat required for regeneration. Since this heat exchanger is between two liquid desiccant streams, the heat transfer coefficients are high and the heat exchanger may be quite compact. After the economizer, the LD is further heated from the regen heat source (solar thermal collector or waste heat) to reach LDP4. The air regeneration stream

49

(AR) is pulled from ambient and heated to match the temperature of LDP4, then both streams enter the regen LAMEE at the same temperature for regeneration. Moisture is removed from the LDP stream and enters the AR exhaust stream (AR2). The process of desorbtion is endothermic and cools the LDP stream (LDP5). The LD then enters the hot side of the economizer and transfers heat to the cold stream (LDP6). Finally LD is cooled back near ambient wet bulb temperature by the reservoir DEC and enters the LD storage tank, this closes the cycle.
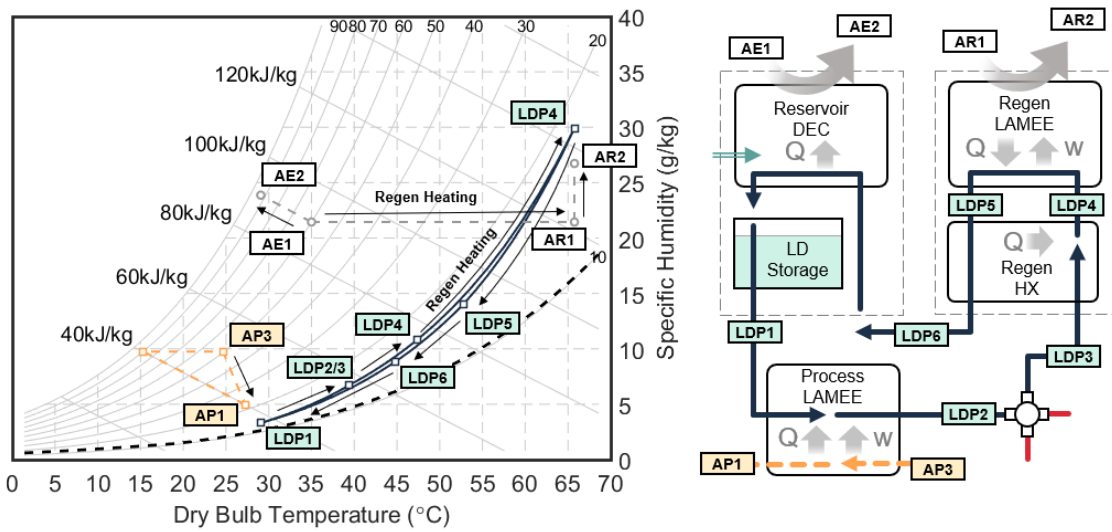
Figure 2-7: LD Process Loop Cycle and Diagram

2.7 Ideal Cycle Limits and Benchmarking

To validate the claim that the DECAL cycle offers thermodynamic advantages over direct supply systems, the ideal cycle performance of several similar systems was evaluated. System 1 comprises a single drying LAMEE followed by a direct evaporative cooler. Ideal performance is assumed for both the LAMEE (sensible and latent effectiveness) and DEC (wet bulb efficiency), and the drying LAMEE inlet condition is set at the solubility limit of the liquid desiccant at the inlet temperature. System 2 consists of a drying LAMEE followed by a dew point cooler (M-cycle). The wet bulb effectiveness is set to 1.20 based on the work of [37] and the ratio of process

air to working air is 1:1. The working stream air for system 2 must also be dried, so the regeneration requirements are doubled relative to a direct evaporative system. However, system 2 does have the advantage of cooler outlet temperatures since it can cool beyond the wet bulb temperature. System 3 is the DECAL system described in this work, with ideal exchanger effectiveness on all exchangers. Indoor temperature is set to 27C and max allowable indoor RH is 60%. The SHR is 0.75. The max indoor RH and SHR imposes an upper limit for systems using direct evaporative cooling. In cases where the cooling stream wet bulb condition falls above the condition line, cooling was limited to the intersection such that SHR is met and the indoor RH is 60%. In cases where the outlet condition falls below the condition line (this mostly applies to system 2) the indoor RH is lowered. This is representative of what would actually occur if latent cooling exceeds the latent load, but does suggest that a dew point cooler system could operate with less drying than shown here.

Each system in the study was assessed both with and without a DEC pre-cooling stage (reservoir DEC in the DECAL system). The ideal thermal coefficient of performance was found for each system using both $CaCl_2$ and LiCl, and over a broad range of ambient conditions (30-45C dry bulb temperature and 20-80% RH). Figure 2-8 shows system diagrams for the process side of each system evaluated, and the cycle of each system on the psychrometric chart at the design condition.

The results are promising for the DECAL system (System 3 with precooling). Figure 2-9 shows contours of the thermal COP limits for each system over the range of ambient conditions evaluated. As expected, performance degrades at higher temperatures and humidities, with some systems falling off faster than others. In general, systems 1 and 2 perform well at very low relative humidity (under 30%). However, at these dry conditions evaporative cooling systems may be used without a desiccant, so performance at higher humidity is of greater interest. DECAL shows capability improvements over much of the range of interest, especially at high ambient temperature and humidity. Both systems 1 and 3 use direct evaporative cooling, so systems with a single stage are limited to the wet bulb temperature corresponding to the solubility limit of the desiccant and ambient temperature. For $CaCl_2$ this occurs just under 40C
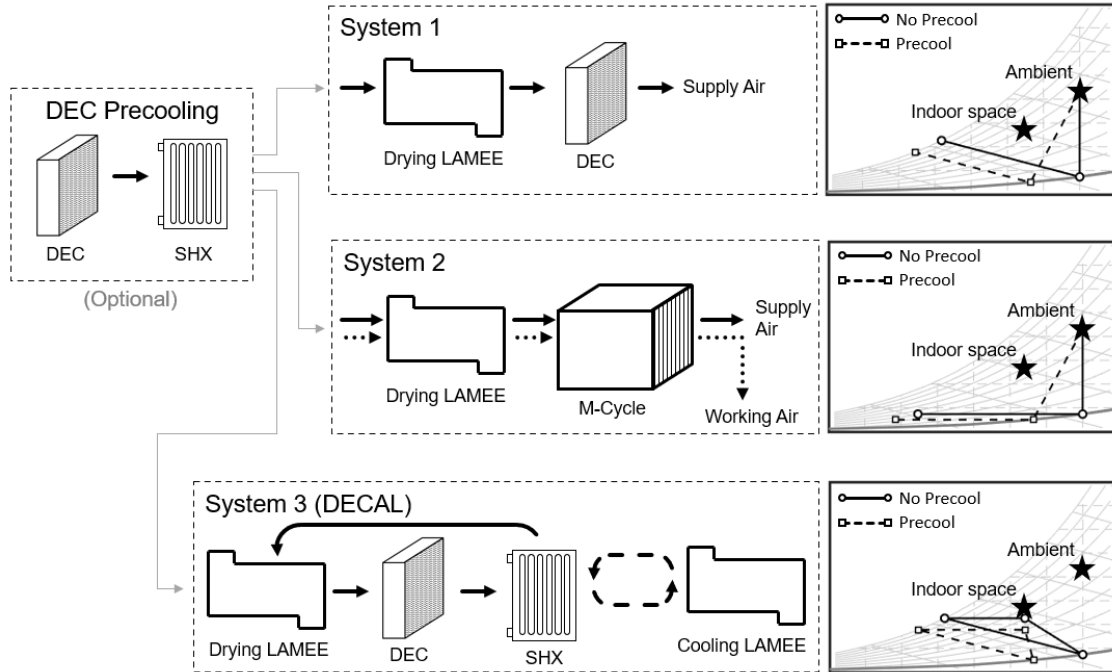
Figure 2-8: System Diagrams for Ideal Limits Studies

ambient dry bulb, so these systems are not viable above that condition, regardless of humidity. Direct comparison between $CaCl_2$ and LiCl shows that with precooling, often $CaCl_2$ outperforms LiCl. This was unexpected since LiCl offers superior drying capacity. It implies that there is an optimal condition at which additional drying is not advantageous i.e. the incremental improvement in cooling capacity over the incremental additional regeneration heat has a maximum. This does not necessarily suggest that $CaCl_2$ will outperform LiCl in a real system since LAMEE latent effectiveness will reduce the actual drying capacity possible, and the lower vapor pressures LiCl offers would allow a smaller exchanger to be used.

While the findings of this study show great promise for the DECAL system, they are incomplete, since actual system performance will vary significantly from the ideal limit. The DECAL system is more complex than the two benchmarks systems it is compared against. This will put more restrictive limits on its performance when component inefficiencies are considered. Actual system performance is investigated extensively with the full system performance model detailed in Chapter 3.
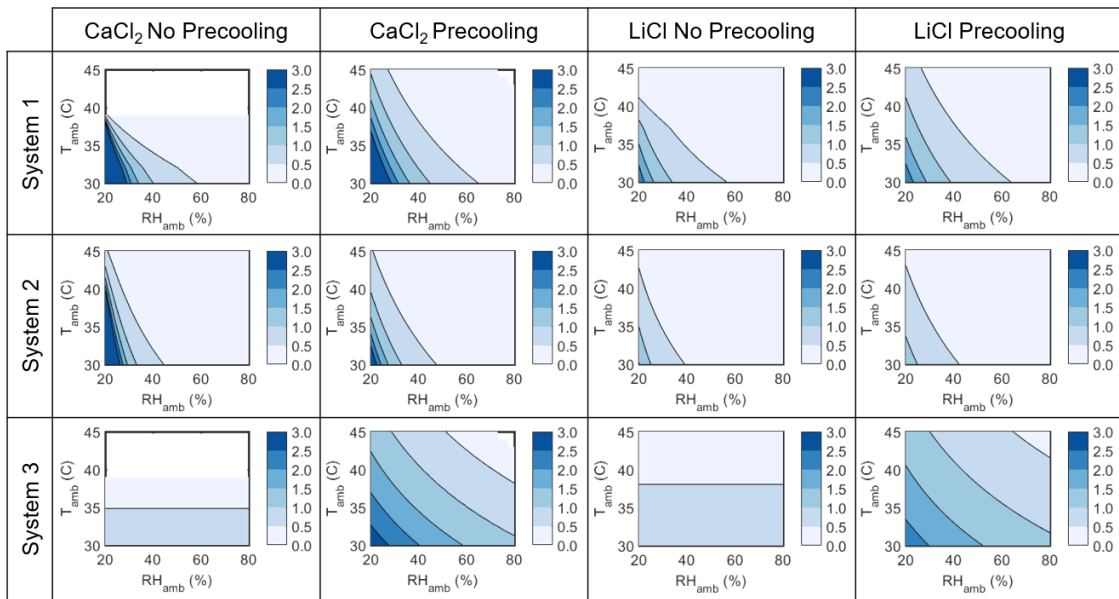
Figure 2-9: Ideal Limits Thermal COP

Chapter 3

Mathematical Model

To simulate system performance, a mathematical model is created using Matlab. The model takes inputs for the indoor and outdoor climate, sensible heat ratio, imposed component efficiencies, liquid desiccant composition (LiCl or CaCl), relative flow rates for each of the fluid loops, and selected geometry constraints. Outputs include cooling power provided, thermal energy and temperature required to regenerate the desiccant, electrical power draw of fans and pumps, and volume required for each exchanger to meet the set efficiencies. The first goal of the simulation is to understand the system limitations with realistic component efficiencies relative to the state of the art. The second goal is to gain insight into the trade-offs between component efficiencies, volume, power, and flow constraints to design a well balanced system. The model is built with a layered architecture of routines and subroutines designed to provide robust and accurate results while maintaining flexibility and speed. Figure 3-1 gives the top-level model architecture for the Matlab model.

The optimization wrapper allows the user to run design studies for various inputs. These inputs may be either boundary conditions such as climate, design parameters such as exchanger efficiencies, or operational settings such as relative flow rates of the fluid loops. The main loop is used to run a single design point. It may be run either as a function called by the optimization wrapper or alone if solving for a single condition. The main loop sets all static parameters needed to solve the system, sets initial guess values for the solver, calls the solver routine, and executes some post-processing
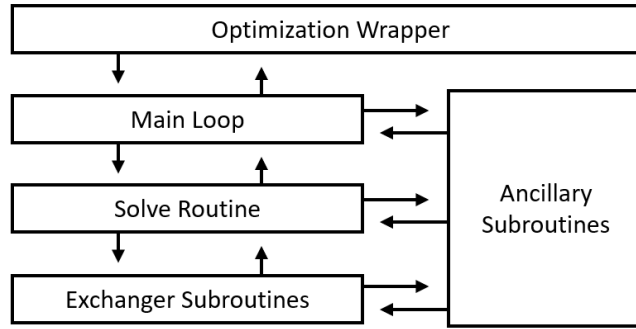
Figure 3-1: Mathematical Model Architecture

for key outputs such as system COP. The solver routine steps through each control volume of the system to fully define each state. Its operation is explained section 3.1. The system consists of six flow-streams in total - two closed liquid desiccant loops, one closed air loop, and three open air loops. At each exchanger, the input states of both streams must first be fully defined, then the appropriate exchanger subroutine is called. Three types of exchangers are used: sensible heat exchangers (SHXs), liquid-air membrane energy exchangers (LAMEEs), and direct evaporative coolers (DECs). The main loop, solver routine, and exchanger subroutines also call ancillary subroutines to define state properties of the fluids, and to set heat transfer and pressure drop relations throughout the solve procedure.

3.1 Solver Routine

The system simulation assumes steady state operation and uniform composition at each station control volume as defined in figure 2-3. The solver steps through each control volume iteratively until the state at each station is fully defined and each conservation equation is satisfied. Liquid desiccant requires two intensive properties to define the state, generally temperature and mass fraction of solute. Humid air requires three properties to fully define the state - two to define the air and a third to define the water vapor content. Although pressure drop does exist in several system components, the changes are small and so the full system is assumed at a constant pressure of 1 atmosphere. Therefore the state of air is fully defined by dry bulb

56

temperature and absolute humidity.

Figure 3-2 shows the steps taken in the solver routine to find the steady state solution. Exchangers and station locations are numbered as shown. The following system parameters are known *a-priori*: indoor and outdoor temperature and humidity, sensible effectiveness for heat exchangers and LAMEEs, and sensible heat ratio of the conditioned space. The indoor state sets a system boundary condition at E5, and outdoor state sets boundary conditions at E1 and E6. The following assumptions are made to facilitate the system solve:

1. The system operates at steady state

2. The liquid desiccant coming from the storage tank at LDP1 is at thermal equilibrium with the reservoir DEC discharge

3. The mixing valve between LDC and LDP streams allows the LDC stream mass concentration to be controlled by exchanging weak and strong liquid desiccant flow

4. The system is thermally isolated from the environment, other than the designated exchangers (E1,E5,E6)

The thermodynamic states at each control volume form a system of non-linear equations which may be solved using the built-in Matlab solver "fsolve". The solver algorithm is set to use *Levenberg–Marquardt*, which interpolates between Gauss-Newton algorithm and gradient descent. The system solve begins by finding the reservoir temperature for the liquid desiccant process stream. Inlet air is at known conditions T_{amb} and ϕ_{amb}. From this the wet bulb temperature is found as defined in section 3.5.1, and the DEC outlet air condition is solved by the DEC subroutine (see section 3.4). Given the assumption that DEC reservoir is in thermal equilibrium with the LDP reservoir, the temperature at LDP1 is set. The mass concentration of liquid desiccant is set by establishing a percentage margin (solubility margin) to the concentration at which salt precipitates from solution (see section 3.5.2). The solubility margin for this study is set to 5%, i.e. the concentration is 95% of the concentration at which it
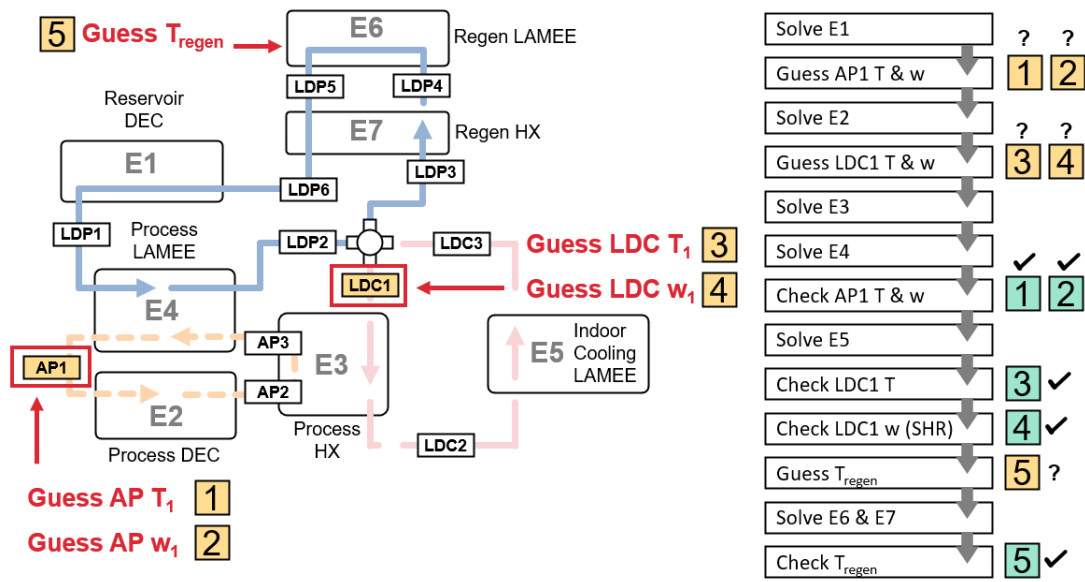
Figure 3-2: System Solver Procedure

precipitates out of solution at the DEC reservoir temperature. For both $CaCl_2$ and LiCl, in the range of temperatures the system encounters the margin to precipitation increases with temperature, so setting the design point at the lowest temperature in the loop ensures the solute never precipitates. None of the conditions of the closed loop process airstream are known *a priori* so both the temperature and humidity ratio at AP1 are guess values. It is important for solver robustness to begin with guess values as close to the converged solution as possible. The guess states for AP1 are set to the same conditions as LDP1 since AP1 is the exit condition of the process LAMEE - therefore if the effectiveness of the LAMEE is high the guesses will be accurate. The state at AP2 is found by calling the DEC subroutine, this station is the cool-side inlet to the process HX. To solve the HX outlet conditions, the hot-side inlet condition must be known. This requires 2 additional guess values for LDC1 T and w. These guesses are set based on the prescribed indoor temperature and humidity. As before, the quality of the guesses is best if LAMEE effectiveness is high. With both inlet streams fully defined the outlet conditions are found by calling the SHX subroutine (see section 3.2 for details). This defines the outlet streams' state at LDC2 and AP3. Next E4 may be solved since LDP1 and AP3 are known, here

58

the exchanger is a LAMEE so the LAMEE subroutine is called (see section 3.3 for details). The outlet conditions of E4 defines LDP2 and provides a check for the AP1 guess values. The relative error term for AP1 temperature is defined in equation 3.1, humidity error is found in a similar way.

$$E_{rel} = \frac{T_{guess} - T_{outlet}}{T_{outlet}} \tag{3.1}$$

The indoor cooling LAMEE (E5) may now be solved since LDC2 and the indoor return air condition are known. This gives the state at LDC3 and the outlet air condition of the indoor cooling LAMEE, which defines the sensible and latent cooling provided. The volume exchange at the mixing valve can now be found by mass conservation of LD solute since mass concentration at LDC1, LDC3, and LDP2 are known. The mixing valve outlet state gives a check on LDC1 temperature guess, but not the LDC1 concentration guess. The mass concentration guess is closed on by checking the outlet SHR from the indoor cooling LAMEE relative to the specified value. Volume exchange at the mixing valve also gives the state at LDP3. Regeneration temperature of the regen LAMEE is guessed, allowing E6 and E7 to be solved and defining LDP4, LDP5, and LDP6. As described in section 2.6, regen heat is applied to both the LD stream and the air stream entering the regen LAMEE. The difference in mass concentration between LDP6 and LDP1 gives the closing parameter for the regen temperature guess and closes the full cycle.

3.2   Sensible Heat Exchanger

3.2.1   Outlet State Calculations

The sensible heat exchanger transfers heat from hot stream to cold stream. There is no mixing, so the composition of inlet and outlet streams are unchanged. Heat transfer between the two streams is given by equation 3.2.

$$q = \varepsilon C_{min} \left(T_{hot\ in} - T_{cold\ in} \right) \tag{3.2}$$

Where ε is the sensible effectiveness and C_{min} is the minimum conductance of the two streams (the product of mass flow and specific heat). Cr, the ratio of conductance between the two streams is set to 1 for each exchanger in the system at the system solve, so $C_{min} = C_{max} = C$. This maximizes the total sensible transfer between streams for a given effectiveness. The effectiveness is specified as an input to the SHX subroutine, so change in temperature of both streams is calculated directly from known inlet conditions by equation 3.3.

$$\Delta T_i = \frac{q}{\varepsilon C_i} = \frac{q}{\varepsilon \dot{m}_i c_{p\,i}} \tag{3.3}$$

3.2.2 Physical Envelope

The volume, face area, and length of the sensible heat exchanger are calculated from the specified effectiveness and face velocity. First the primary surface area is back-calculated from the effectiveness-NTU method. The two sensible heat exchangers in the system are treated differently since the process HX takes air and LD while the economizer exchanges between two LD streams. Both SHXs are counterflow configuration. The process HX is treated as a radiator with LD flow through flattened tube headers and no internal extended surfaces. The air side has fins formed by thin corrugated sheet metal based on the hardware used in the experimental setup. The air-side channel geometry approximation is shown in figure 3-3.

The number of transfer units (NTUs) can be found for a counterflow heat exchanger by equation 3.4 [10].

$$NTU = \frac{1}{C_r - 1} \ln \left(\frac{\varepsilon - 1}{\varepsilon C_r - 1} \right) \tag{3.4}$$

When $C_r = 1$, this simplifies to equation 3.5 [10].

$$NTU = \frac{\varepsilon}{1 - \varepsilon} \tag{3.5}$$

Total conductance between the hot and cold side of a heat exchanger is the inverse of the total thermal resistance between the two streams. In a direct-transfer

60
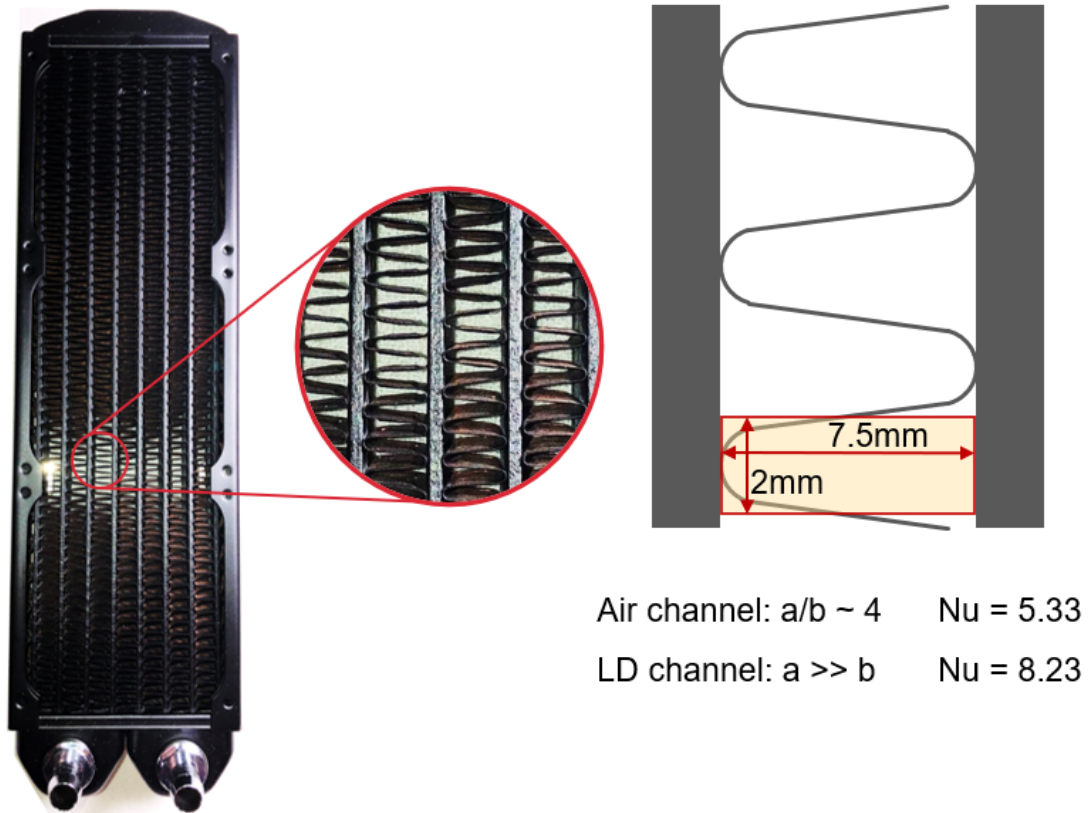
Figure 3-3: Process SHX Air Side Channel Geometry

heat exchanger this resistance may be broken down to three components, the convective resistance on hot and cold sides, and the conductive resistance across the wall separating the streams. The conductance between sides 1 and 2 from the perspective of side 1 is defined below in equation 3.6.

$$U_1 A_1 = \cfrac{1}{\cfrac{1}{\eta_{o1} h_1 A_1} + R_w + \cfrac{1}{\eta_{o2} h_2 A_2}} \qquad (3.6)$$

In a finned radiator as described above, the area on the air-side is not equal to the area on the liquid side. Since total heat transfer goes with the sum UA and must be equal on both sides, the overall heat transfer coefficient differs between the finned side and the unfinned side. Since the fin spacing and geometry is known, the finned side area A_f may be related to the unfinned (primary) side area A_p by equation 3.7.

$$\chi_f = \frac{A_p + A_f}{A_p} = 1 + \frac{2b}{s} \tag{3.7}$$

Where b is the length the fin extends from the base and s is the fin spacing. Based on figure 3-3, $s = 2$mm and $b = 3.75$mm, it is assumed that the fin length is half the air channel width, i.e. adiabatic at the center line. With this equation known, equation 3.6 can be simplified. Furthermore, it is assumed the wall resistance is negligible relative to the convective resistance. Therefore the simplified conductance equation is given by 3.8.

$$U_1 = \frac{1}{\dfrac{1}{\eta_{o1} h_1} + \dfrac{\chi_f}{h_2}} \tag{3.8}$$

Where η_{o1} is the overall surface efficiency of the finned side as defined in equation 3.9.

$$\eta_o = 1 - \chi_f \left(1 - \eta_f\right) \tag{3.9}$$

Here η_f is the fin efficiency, which can be found by equation 3.10.

$$\eta_f = \frac{tanh(mL)}{mL} \tag{3.10}$$

The fin efficiency may be found from physical properties of fin, since $m = \sqrt{\frac{2h}{kt}}$.

The convective heat transfer coefficient h on each side of the exchanger is found from the Nusselt number, which is constant for fully developed flow with uniform heat flux. 3.11 [10].

$$Nu = \frac{hD_h}{k_f} \tag{3.11}$$

Where D_h is the hydraulic diameter of the passage and k_f is the thermal conductivity of the fluid. In passages with large aspect ratios (channel width » channel height) $Nu = 8.23$ - this value is used for liquid side channels. In air side channels,

the aspect ratio (width/height) is approximately 4, so $Nu = 5.33$ is used [10].

By the preceding method, the primary surface area of the exchanger is found from imposed conditions on the air side. The volume of the exchanger is then found by

$$V_{SHX} = A_p \frac{g_1 + g_2}{2} \tag{3.12}$$

Where g_1 and g_2 are gap widths of of the two fluid streams and A_p is the primary surface area as described above. SHX air channels are set to 7.5mm and liquid channels are set to 2mm based on dimensions of the experimental hardware. The face velocity and volume flow are specified as inputs, so the face area may be determined directly from these inputs. Furthermore, once the volume is solved, it is trivial to solve the length of the exchanger. The aspect ratio for each exchanger is also found, based on its definition in equation 3.13.

$$AR = \frac{L}{\sqrt{FA}} \tag{3.13}$$

3.2.3 Pressure Drop and Power Draw

To determine the fan and/or pump power required for the heat exchanger, first the pressure drop for both streams must be calculated. The channel velocity on the air side is specified, so the Reynolds number may be calculated directly by equation 3.14. Channel velocity on the LD side is found from volume flow, channel height, and the face area on the air side, assuming both channels are equal width from the air-side face.

$$Re_i = \frac{\rho_i u_{ch\ i} D_{h\ i}}{\mu_i} \tag{3.14}$$

Where ρ_i is density, $D_{h\ i}$ is hydraulic diameter, and μ_i is the dynamic viscosity of the stream of interest.

Pressure drop consists of major losses and minor losses, where major losses occur due to friction along the length of the channel and minor losses occur at bends, expansion/contractions, or other features which could cause flow separation. Major

losses are found using the Darcy-Weisbach equation (3.15) [20].

$$\Delta P_{maj} = f\frac{Lu_{ch}^2\rho}{2D_h} \tag{3.15}$$

Where L is the length of the duct, u_{ch} is average channel velocity, ρ is the density of the fluid, D_h is hydraulic diameter, and f is the friction factor. For laminar flow, the friction factor is defined by equation 3.16. When flow is turbulent, f must be found iteratively by the Colebrook equation (3.17) [20].

$$f = \frac{64}{Re} \tag{3.16}$$

$$\frac{1}{\sqrt{f}} = -2\,log\left(\frac{e/D}{3.7} + \frac{2.51}{Re\sqrt{f}}\right) \tag{3.17}$$

Here e/D is the relative roughness - surface roughness over hydraulic diameter of the channel. For the smooth surface of the SHX, the relative roughness is set to 0.001.

The only minor losses considered are the entrance and exit losses between exchangers. These are defined by 3.18

$$\Delta P_{min} = K\frac{\rho u_{ch}^2}{2} \tag{3.18}$$

Where K is the loss coefficient. K = 0.5 for both entrance and exit loss for a square edged inlet/exit.

Neglecting heat transfer and internal energy changes in the fluid, and assuming no change in height or velocity between inlet and exit, the fan power is given by equation 3.19.

$$P_{fan\ ideal} = \dot{v}\Delta P \tag{3.19}$$

Where $\dot{v}$ is the volume flow and ΔP is the pressure drop. To calculate actual power consumption, the fan efficiency η_{fan} must be considered, see equation 3.20.

$$P_{fan\ actual} = \frac{P_{fan\ ideal}}{\eta_{fan}} \qquad (3.20)$$

Pump power for fluid streams is calculated in the same way. Fan efficiency is assumed at 70% and pump efficiency is assumed constant at 50%, both estimates are conservative.

3.3 Liquid-Air Membrane Energy Exchanger

3.3.1 Outlet State Calculations

The LAMEE subroutine performs many of the same calculations as the SHX subroutine, but includes mass transfer in addition to heat transfer. The following assumptions are made to bound the problem.

1. Flow streams in the LAMEE are one-dimensional in counter-flow orientation

2. Fluid flow is fully developed

3. The system is in steady state operation

4. Conduction and diffusion along the length of the LAMEE are negligible

5. The temperature change due to heat of adsorption or desorption occurs on the liquid side

Furthermore it is assumed that changes in mass flow due to moisture exchange between air and LD streams is small relative to the overall mass flow. It follows that the change in mass concentration of the LD is also small and so thermodynamic and transport properties may be taken at the inlet of the LAMEE. This avoids the need for an iterative solution on outlet properties.

All sensible heat transfer is calculated the same as in the SHX subroutine, with the following exceptions.

1. There are no fins in the LAMEE, all exchange is through the primary surface

2. The flow spacers reduce the exchange area by a non-negligible amount, this reduction must be accounted for in the physical envelope calculations

3. Additional heat gain occurs due to absorption of water vapor, this is added to the liquid desiccant side of the energy balance in outlet condition calculations

As before, the sensible effectiveness of the LAMEE is prescribed, so heat transfer due to sensible exchange may be calculated by 3.2. The latent effectiveness of a LAMEE is defined by Navmar [34] and Ge [21] in equation 3.21.

$$\varepsilon_L = \frac{W_{air\ in} - W_{air\ out}}{W_{air\ in} - W_{sol\ in}} \tag{3.21}$$

Since the latent effectiveness is a function of other properties of the LAMEE which are specified, it must be calculated from NTU relations. The latent NTU relation for a counterflow LAMEE is given by equation 3.22 [34].

$$\varepsilon_{L\ counterflow} = \frac{1 - exp - (NTU_m(1 - m^*))}{1 - m^* exp\left(-NTU_m(1 - m^*)\right)} \tag{3.22}$$

Here NTU_L is defined by equation 3.23

$$NTU_L = \frac{U_m SA}{\dot{m}_{min}} \tag{3.23}$$

Where U_m is the overall mass transfer coefficient, SA is the total surface are of the exchanger (found from the prescribed sensible effectiveness), and $\dot{m}_{min}$ is the smaller mass flow rate entering the exchanger (air or liquid desiccant). m^* in equation 3.22 is the ratio between the lower mass flow rate and the greater mass flow rate entering the exchanger [34].

Similar to the overall heat transfer coefficient in section 3.2, the overall mass transfer coefficient is found by eqn. 3.24, where $h_{m\ sol}$ is the convective mass transfer coefficient of the LD stream, $h_{m\ air}$ is the convective mass transfer coefficient of the air stream, δ is the membrane thickness, and k_m is the membrane water vapor transmission resistance, a value of 24 s/m is used for this parameter based on prior studies [27] [22].

$$U_m = \left[\frac{1}{h_{m\ sol}} + \frac{\delta}{k_m} + \frac{1}{h_{m\ air}} \right]^{-1} \tag{3.24}$$

The convective mass transfer coefficient is related to the convective heat transfer coefficient by equation 3.25, derived from the Chilton-Colburn analogy [21]. A Lewis number (Le) of 1 is used for this work.

$$h_m = \frac{h}{c_p} Le^{-2/3} \tag{3.25}$$

By the methods described above, the exchanger mass transfer and outlet states are calculated from imposed exchanger properties and inlet states of both fluid streams.

3.3.2 Physical Envelope

Physical envelope of the exchanger is found in the same manner as the SHX, but without the complication of extended surfaces. The LAMEE does require flow spacers on both air and fluid sides to prevent flow maldistribution due to bulging of the membrane. This reduces the effective surface area where the spacer blocks the membrane on either the air side or LD side. Thus, the actual required envelope is slightly greater than the primary surface area would suggest. To account for this, the effective surface area is defined.

$$SA_{eff} = SA - (B_{LD} + B_{air}) \tag{3.26}$$

Where B_{LD} is the blockage area on the liquid desiccant side and B_{air} is the blockage area on the air side. Based on measured blockages on the experimental unit, the LD and air blockages are 9% and 10%, respectively, so $SA_{eff} = 81\%\ SA$.

3.3.3 Power Draw

LAMEE power draw is found in the same way as sensible heat exchanger power draw. It consists of fan power for the air stream and pump power for the LD stream. The same isentropic efficiencies are used for fan and pump. Length on the air side

is found from the effective surface area in equation 3.26. The LD side flows in a switch-back configuration as described in section 4.2.3, so the flow channel width is constant $W_{ch} = 44mm$ and the number of switchbacks depends on the exchanger length: $n_{turns} = \frac{L}{W_{ch}}$. Total length of the LD side channel is the number of turns multiplied by the width of the air side channel.

3.4 Direct Evaporative Cooler

3.4.1 Outlet State Calculations

Direct evaporative coolers generate a sensible cooling effect through evaporation of water. The most common configuration uses a pad of durable corrugated paper, known as evaporative media, as the heat and mass transfer surface. Water is dripped slowly on top of the pad and travels by gravity and capillary action to a collection basin at the bottom of the device and recirculated by a small water pump. Air is blown through the pad by a fan or blower, causing some of the water to evaporate.

It is assumed that the system is thermally isolated from the environment, so parasitic heat gain may be neglected. The water supply is recirculated so that the water flowing into the evaporative media is just above the wet bulb temperature of the air. The only net heat flow into the system from the water supply is due to the temperature difference between the wet bulb temp and the supply temp which at worst will be ambient, but may be cooler if supplied by an underground municipal water supply. Since this heat gain is proportional to, and much smaller than, the sensible removal ($h_{vap} >> c_p \Delta T$), it is neglected. With the above assumptions, the process may be treated as constant enthalpy, so that any sensible heat removed from the air is gained as latent heat.

The saturation efficiency or wet bulb effectiveness of the DEC is defined by eqn. 1.6 where t_{in} is the inlet air dry bulb temp, t_{out} is the outlet air dry bulb temp, and t_{wb} is the wet bulb temp of the inlet air-stream.

68

3.4.2 Physical Envelope

The physical envelope of the DEC is found directly from the face area and length. The face area comes directly from the volume flow and channel velocity, and the length is determined from the requisite wet bulb effectiveness. Wu [43] studied wet bulb effectiveness of direct a evaporative cooler with a similar evaporative pad at flow rates between 1 and 4 m/s and validated results with experimental data. They established the relation in equation 3.27 which concisely relates properties of the evaporative pad and frontal velocity to estimate wet bulb effectiveness of the DEC.

$$\eta_{wb} = 1 - \exp\left(\frac{-\alpha L}{u^{.35}}\right) \tag{3.27}$$

Where L is the length of the pad in the direction of flow, u is the frontal velocity, and alpha is given by

$$\alpha = \frac{A\xi}{\rho c_p} \tag{3.28}$$

Here ξ is the pore surface coefficient or surface area per volume, ρ is the density of air, c_p is the specific heat of air, and A is an empirical coefficient unique to the pad material and configuration, which is similar to the type used here. The geometry of the pad used in this study is similar to the CELdek7090 used in [43], so the value of ξ from that study (440 $m2/m3$) is used here. To find volume and pressure drop, the length of the exchanger is found by rearranging equation 3.27 and solving for L.

3.4.3 Power Draw

Unlike the sensible heat exchanger and LAMEE, flow in the DEC is not fully developed. Shah [39] gives a method for determining pressure drop of developing flow for several duct geometries. Dimensionless length is found by equation 3.29.

$$x^+ = \frac{L}{D_h Re} \tag{3.29}$$

Where L is the length of the duct and D_h is hydraulic diameter. Next the product

of apparent friction factor and Reynolds are found by equation 3.30.

$$f_{app}Re = \frac{3.44}{\sqrt{x^+}} + \frac{fRe + K/(4x^+) - 3.44/\sqrt{x^+}}{1 + C(x^+)^{-2}} \tag{3.30}$$

Here $K = 1.69$, $fRe = 13.333$, and $C = .00053$. These empirical constants apply for developing flow in a triangular duct. The dimensionless pressure drop may then be found by equation 3.31.

$$\Delta P^* = (f_{app}Re)(4x^+) \tag{3.31}$$

Finally, the pressure drop is calculated by equation 3.32.

$$\Delta P = 1.1\Delta P^* \frac{\rho u^2}{2g_c} \tag{3.32}$$

Where ρ is density, u is flow velocity, g_c is the gravitational constant 9.81 m/s^2, and 1.1 is a factor included to account for surface wetting [11]. Once pressure drop is found, fan power required by the DEC is calculated in the same way as the SHX and LAMEE subroutines.

3.5   Ancillary Subroutines

3.5.1   Air State Calculations

Air psychrometric calculations to give dry bulb temperature T_{db}, humidity ratio w, relative humidity ϕ, dew point temperature T_{dp}, and wet bulb temperature T_{wb} are summarized in this section. The calculations follow the approach given in sections 4-8 of the 2017 ASHRAE Handbook Fundamentals. [5]

The humidity ratio w is the ratio of the mass of water vapor to dry air M_w/M_{da}.

The saturation pressure p_{ws} in Pa is calculated from the temperature in K using eqn. 3.33, valid on the range 0-200C.

$$ln(p_{ws}) = C_1/T + C_2 + C_3T + C_4T^2 + C_5T^3 + C_6ln(T) \tag{3.33}$$

Where

$$C_1 = \text{-5.8002206 E3} \qquad C_3 = \text{-4.8640239 E-2} \qquad C_5 = \text{-1.4452093 E-8}$$

$$C_2 = 1.3914993 \qquad C_4 = \text{4.1764768 E-5} \qquad C_6 = 6.5459673$$

The humidity ratio is related to the saturation pressure by equation 3.34. In this study the ambient pressure p is assumed constant at 101325 Pa.

$$W = 0.621945 \frac{p_w}{p - p_w} \tag{3.34}$$

The saturation humidity ratio is defined in equation 3.35.

$$W_s = 0.621945 \frac{p_{ws}}{p - p_{ws}} \tag{3.35}$$

The relative humidity ϕ is the ratio of the partial pressure of water vapor in the air to the saturation partial pressure as defined above. Given these relations, the humidity ratio may be calculated given the dry bulb temperature and relative humidity, or the relative humidity may be calculated given the dry bulb temperature and humidity ratio.

The dew point temperature is calculated below in equation 3.36, valid from 0-93C. Here the partial pressure of water p_w is in kPa.

$$T_{dp} = C_1 + C_2\alpha + C_3\alpha^2 + C_4\alpha^3 + C_5(p_w)^{0.1984} \tag{3.36}$$

Where

$$\alpha = ln(p_w) \qquad C_2 = 14.526 \qquad C_4 = 0.09486$$

$$C_1 = 6.54 \qquad C_3 = 0.7389 \qquad C_5 = 0.4569$$

The thermodynamic wet bulb temperature T_{wb} is the temperature at which water evaporated adiabatically into air will bring it to saturation at the same temperature and pressure. Conservation of enthalpy gives equation 3.37.

$$h + (w_s^* - w)h_w^* = h_s^* \tag{3.37}$$

Where h is the initial enthalpy of the air, h_w^* is the enthalpy of the water added, and h_s^* is the saturation enthalpy of the mixed air, w and w_s^* are the initial and saturation humidity ratio of the air.

Substituting the ideal gas relation and solving for humidity ratio gives equation 3.38.

$$w = \frac{(2501 - 2.32t_{wb})w_s^* - 1.006(t - t_{wb})}{2501 + 1.86t - 4.186t_{wb}} \tag{3.38}$$

Therefore given T_{db} and ϕ, the wet bulb temperature may be found iteratively using equations 3.35 and 3.38 [5].

3.5.2 Liquid Desiccant State Calculations

Accurate liquid desiccant state calculations are critical to understand and predict behavior of the LAMEE. Conde [15] conducted an extensive literature review of over 100 works from 1850 onward and derived empirical relations for each of the relevant thermophysical properties of LiCl and $CaCl_2$. Each property may be found from solute concentration and temperature over the range of temperatures of interest for this study. For the sake of brevity, the detailed calculations are not shown here, but Table 3.5.2 summarizes each of the properties calculated and inputs required.

Property	Calculated From	Used For
Saturation Limit	W	Solubility margin calculations
Vapor Pressure	T,W	LAMEE mass transfer calcs
Density	T,W	LAMEE envelope calcs (volume flow)
Viscosity	T,W,ρ_{H2O}	LAMEE pressure drop calcs (Re)
Enthalpy of Dilution	T,W	Heat of mixing in mixing valve
Diffusion Coefficient	T,W,μ,ρ	LAMEE mass transfer calcs

Perhaps the two most important state properties of the liquid desiccant are the saturation limit, which sets the range of temperatures over which a given mass concentration of LD may operate, and vapor pressure, which determines the equilibrium

relative humidity at a given mass concentration and temperature. Both properties are shown for $CaCl_2$ and LiCl in figure 3-4 as an overlay on the psychrometric chart.
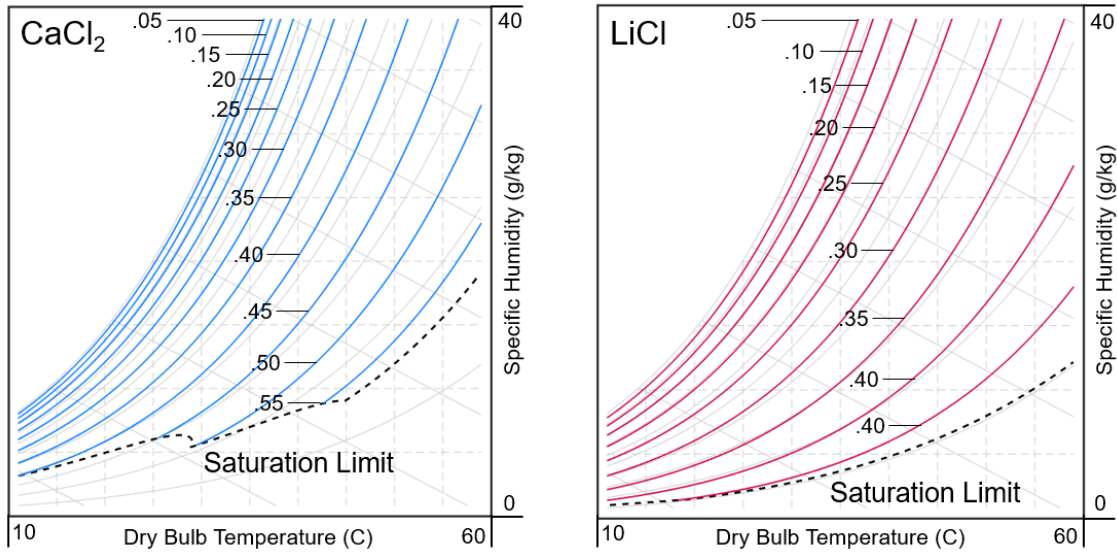

Figure 3-4: Liquid Desiccant and Water Vapor Equilibrium - $CaCl_2$ and LiCl

Lines of constant mass concentration roughly follow lines of constant relative humidity, with higher concentrations at equilibrium with lower relative humidity. Since a higher concentration is desirable to produce a greater drying effect, LiCl is generally preferred between the two desiccants in spite of its higher cost.

3.6   Model Results

3.6.1   Exchanger Efficiency Sweep

As a first check to gain understanding of system performance relative to the figures of merit defined in table 2.2 and assess basic viability of the DECAL cycle, an efficiency sweep was performed. Each of the seven exchangers was set to the same base efficiency (wet bulb effectiveness for DECs, sensible effectiveness for SHXs and LAMEEs) over the range 0.75-0.95. Results are given in figure 3-5.

Here the shaded orange section shows where the design space is limited based on the requirements. General trends follow intuition, as exchanger efficiency increases
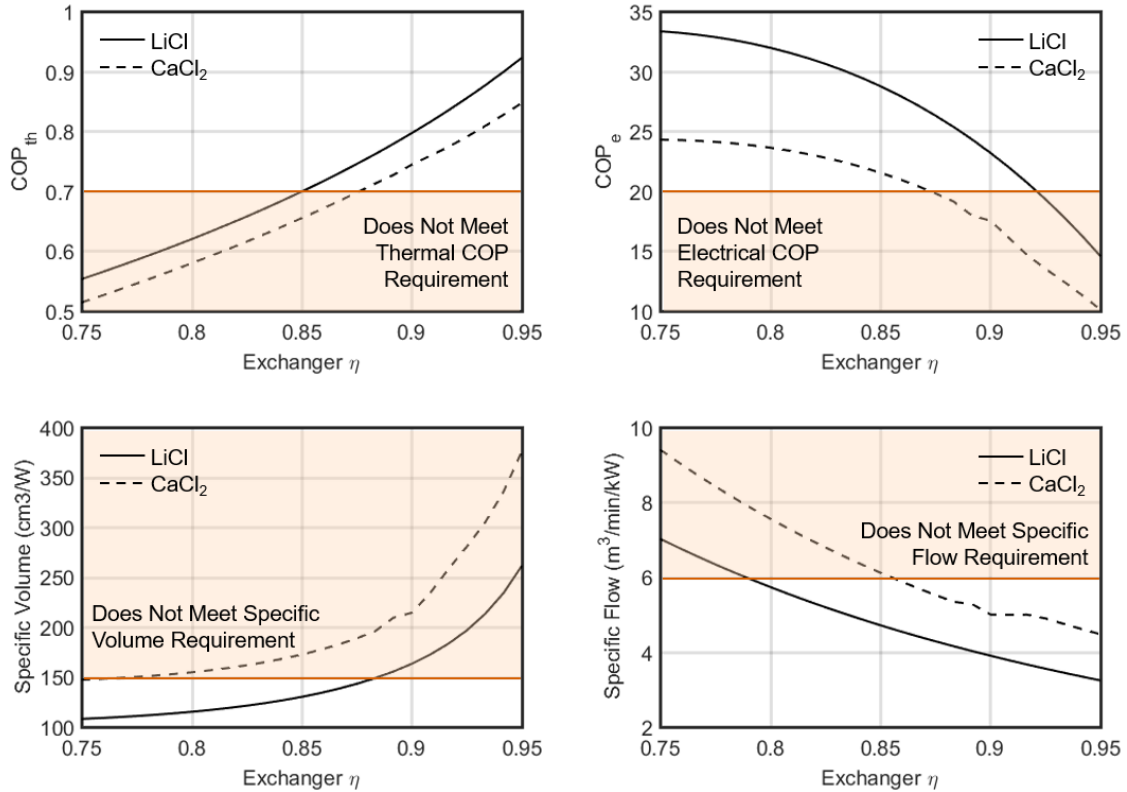
Figure 3-5: System Figures of Merit vs Exchanger Efficiency

so does thermal COP, but electrical COP drops due to the accompanying increase in pressure drop with larger exchangers. As exchanger efficiency increases so does system volume, but as efficiency increases, less volume flow is required to achieve a given cooling output. The relative behavior of the two desiccants is as expected - the less capable $CaCl_2$ gives lower thermal and electrical COPs, and requires larger volume and more flow to achieve the same cooling. The specific volume requirement appears to be the most prohibitive requirement, and is especially difficult to meet for $CaCl_2$ systems. There is a small window between approximately 0.85 and 0.88 in which the LiCl system meets all design requirements, with the left bound on thermal COP and the right bound on specific volume. None of the $CaCl_2$ systems meet all requirements in this initial assessment.

3.6.2 Design Space Exploration

While the exchanger efficiency sweep provides meaningful insight for performance trends, it is limited to designs in which all efficiencies are equal. A balanced system design requires each component efficiency to be tuned to deliver the best performance toward the design targets. To achieve this balanced design, a Monte-Carlo assessment is conducted in which each of the exchanger efficiencies is independently varied. The study is conducted at the standard climate condition given in table 2.1 - 35C 60% RH outdoors, 27C 60% RH indoors, SHR = 0.75. Furthermore, the air gap in the exchangers is held constant at 2mm, fan and pump isentropic efficiencies are set to 70% and 50% respectively, and air channel velocity is set to 3 m/s.

To select the optimal design, the overall system figure of merit is defined in equation

$$FOM_{sys} = \frac{\hat{COP}_e \ \hat{COP}_{th}}{\hat{Vol} \ \hat{v}} \tag{3.39}$$

Where each parameter is normalized to its target value. This gives equal weighting to each figure of merit, assuming the target value is met. To establish the range over which each parameter should be varied, several small sub-studies were completed with sample sizes between 100-500. Once ranges were established, a 10,000 point run was completed for both LiCl and CaCl$_2$ designs. The efficiency ranges tested are given below in table 3.6.2.

Exchanger	Function	η_{min}	η_{max}
E1	Reservoir DEC	.85	.95
E2	Process DEC	.90	.95
E3	Process SHX	.70	.90
E4	Process LAMEE	.70	.85
E5	Cooling LAMEE	.70	.90
E6	Regen LAMEE	.70	.85
E7	Economizer	.70	.85

Table 3.1: Range of Efficiencies Used in Design Exploration Study

Table 3.6.2 shows the percentage of designs meeting each of the requirements individually, and the percentage which met all requirements. Thermal COP was the most limiting for both desiccants, and specific flow was restrictive for $CaCl_2$ but not LiCl.

	CaCl$_2$	LiCl
Percentage of test points converged	97.7	95.5
Percentage of converged designs meeting volume requirement	81.8	100
Percentage of converged designs meeting flow requirement	26.0	100
Percentage of converged designs meeting COP$_e$ requirement	99.9	100
Percentage of converged designs meeting COP$_{th}$ requirement	11.2	33.6
Percentage of converged designs meeting all requirements	8.8	33.6
Optimal design figure of merit	2.61	7.03

Table 3.2: Design Exploration Study Requirements Summary

Figure 3-6 shows the full results dataset for both desiccants plotted against each of the figures of merit. Light-colored points are evaluated, but do not meet one of the four design targets, dark-colored points meet all design targets. The selected design, based on the system figure of merit in equation 3.39, is plotted as well.

	CaCl$_2$	LiCl
Specific Volume (cm^3/kW)	103.4	74.9
Specific Flow (m^3/min/kW)	4.99	4.29
COP$_e$	33.2	46.3
COP$_{th}$	.707	.759

Table 3.3: Optimized Design Performance at Design Point

LiCl outperforms $CaCl_2$ in every category, though the extent of the difference in performance suggests $CaCl_2$ still warrants consideration in the DECAL system due to its lower cost. Further studies are needed to evaluate the economic trade-offs of the system. Both desiccants show promising performance on electrical COP, exceeding
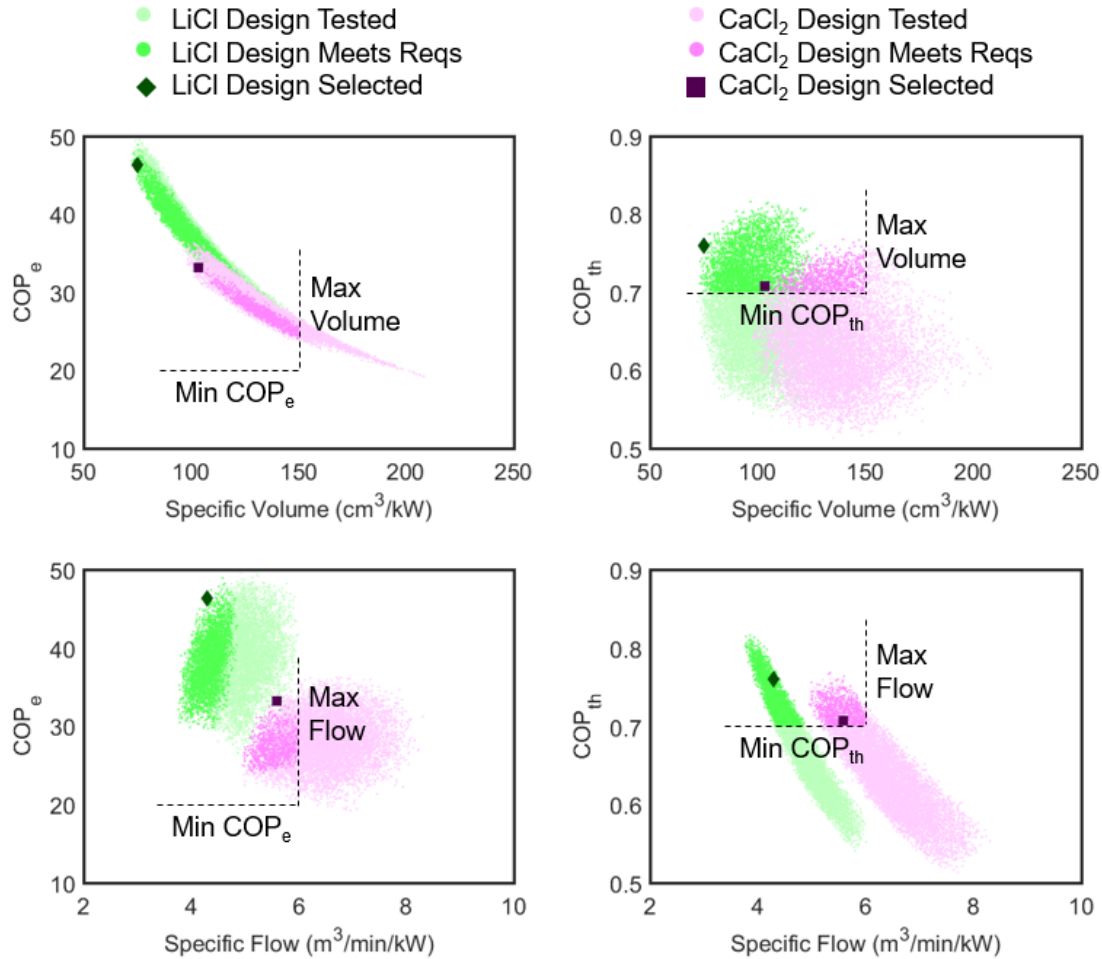
Figure 3-6: Design Exploration Results

the target by as much as 130%. On the other hand, the specific flow and specific volume both present challenges. While the system does show the ability to meet the chosen targets, these targets were set beyond the present day state of the art. Specific volume is less of a concern, since both LiCl and CaCl$_2$ units are within the range of commercially available units today. However, the volumes calculated in this study only consider the exchangers themselves, not any additional volume required for fans, pumps, electronics, or ducting. This could increase the envelope of the final product considerably, and calls for further investigation. Specific flow of modern mini-split units is around 3 m^3/min/kW, whereas the design study shows the lowest feasible flow for a LD system is around 4. This would imply the indoor unit will either need to increase flow velocity, which reduces its electrical performance and increases noise,

or increase the size of the indoor unit, which drives cost and reduces installation flexibility.

Chapter 4

Experimental Validation

The full DECAL system proposed in this thesis consists of 7 exchangers, 2 closed liquid desiccant loops, 1 closed air loop, and 3 open air loops. A full-scale demonstration of the complete system was beyond the scope of this effort, so experimental validation was limited to a small scale demonstration of the closed air loop in the process module. The process module is the heart of the DECAL system and carries the greatest technical risk. This chapter summarizes the experimental work that was done to demonstrate performance of the system and validate the mathematical model.

4.1 Covid19

It is prudent at this point to briefly note how the Covid19 pandemic affected the experimental segment of this research. MIT labs shut down on-site research in March 2020, just before testing was scheduled to begin, and remains at reduced capacity at the time of writing. For this reason, all testing was conducted off-site at own residence. I want to thank the MechE department, Doug Hart, Dan Herrick, and Pierre Lermusiaux for working with me to ensure a safe and successful, albeit unconventional testing experience. In addition to the MIT lab ramp down, the pandemic affected the ability to source hardware due to shipping delays and priority for PPE production. As an example, the LAMEE was originally designed to be lasercut from acrylic in an MIT makerspace. Due to the pandemic, the lasercutting had to be

outsourced, and PETG was substituted for acrylic which was being used to make face-masks for healthcare workers. Testing off site put restrictions on the control and instrumentation of the test rig. Since lab equipment was not available the control and instrumentation of the test was limited to hardware that could be sourced and operated in a "home lab". While great care was taken to ensure reliable and repeatable data, compromises were necessary due to the circumstances. It is my hope that further development and testing of the DECAL system may continue at MIT once normal operation resumes.

4.2   Test Rig Design

The test rig includes the process DEC, the process HX, and the process LAMEE - in this chapter referred to as the DEC, the SHX, and the LAMEE. These three exchangers allow the process air to complete a full closed loop, but since the rest of the hardware is not included, only the first two stations of LDC and LDP loops are represented in the test. Figure 4-1 shows a block diagram of the test rig showing how LDC and LDP loops were truncated. Since air in the process loop never mixes with other air-streams, the inputs and outputs to the system are liquid desiccant. This simplifies the testing significantly, since the input tanks can be easily maintained at temperature rather than requiring an environmental chamber which maintains temperature and humidity. Furthermore, since the LDC loop exchanges only sensible heat with the process air, water was used instead of liquid desiccant with corrections for conductance and density.

Practical limitations on hardware size set the bounding envelope for the benchtop test. The width of the LAMEE was set by the width of the membrane roll (270mm), and the length (680mm) was set by the envelope of the laser cutter and the overall desired length of the rig. Liquid desiccant leakage in the LAMEE was identified early as a key risk, so the number of membrane plates was kept to a minimum. This resulted in a tall and narrow face similar to other flat plate LAMEEs in the literature [21][27][34]. In a closed air loop it is ideal for the face profile to remain
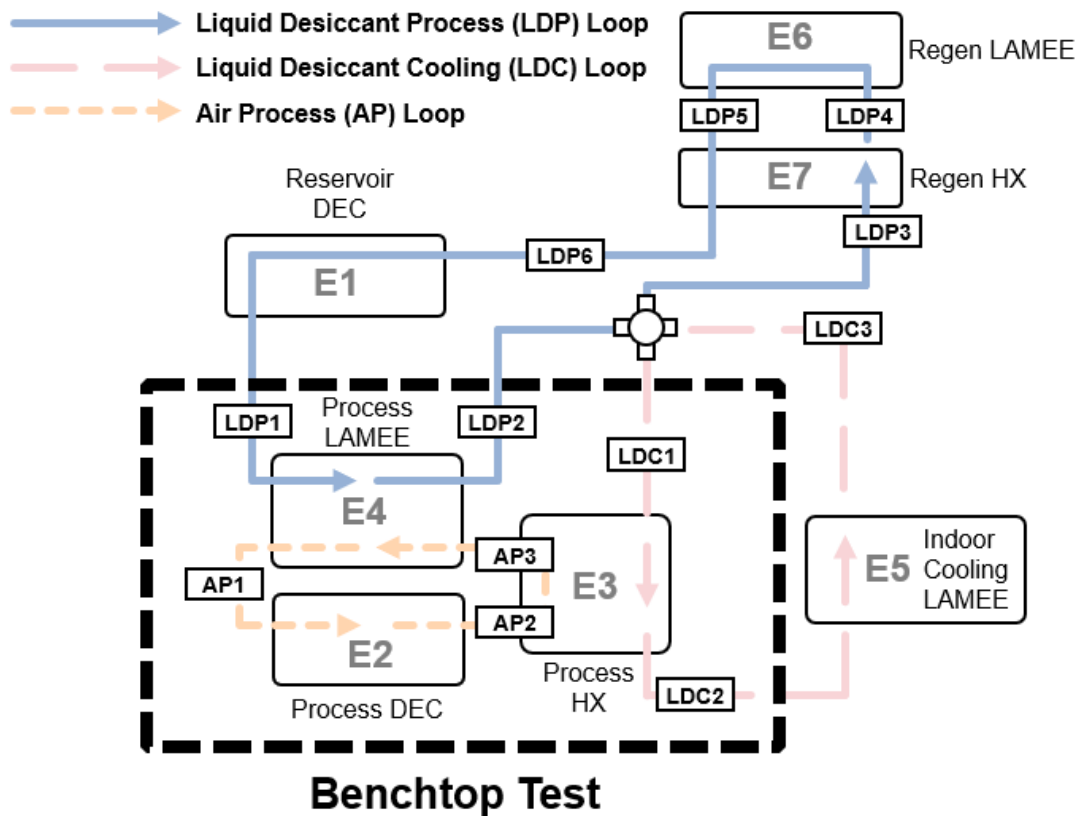
Figure 4-1: Benchtop Test Block Diagram

relatively constant to minimize wasted volume and pressure drop from expansions and contractions in ducting. Therefore, the SHX and DEC face profiles were set to be compatible with the LAMEE. The fans used to move air through the system also added a constraint. Axial fans were used since they are efficient and easy to source. A stacked arrangement of 3 80mm x 80mm fans matched the width of the LAMEE face and the heat exchangers. The small scale of the benchtop test made it easier to source hardware and allowed 3D printed ducts and adapters to be used throughout the testing phase.

4.2.1 DEC Module Design

The DEC is the exclusive source of cooling in the DECAL benchtop test system, so it is crucial to achieve the greatest possible temperature change in this module. The system is designed to maximize wet bulb effectiveness even at high flow velocities. The
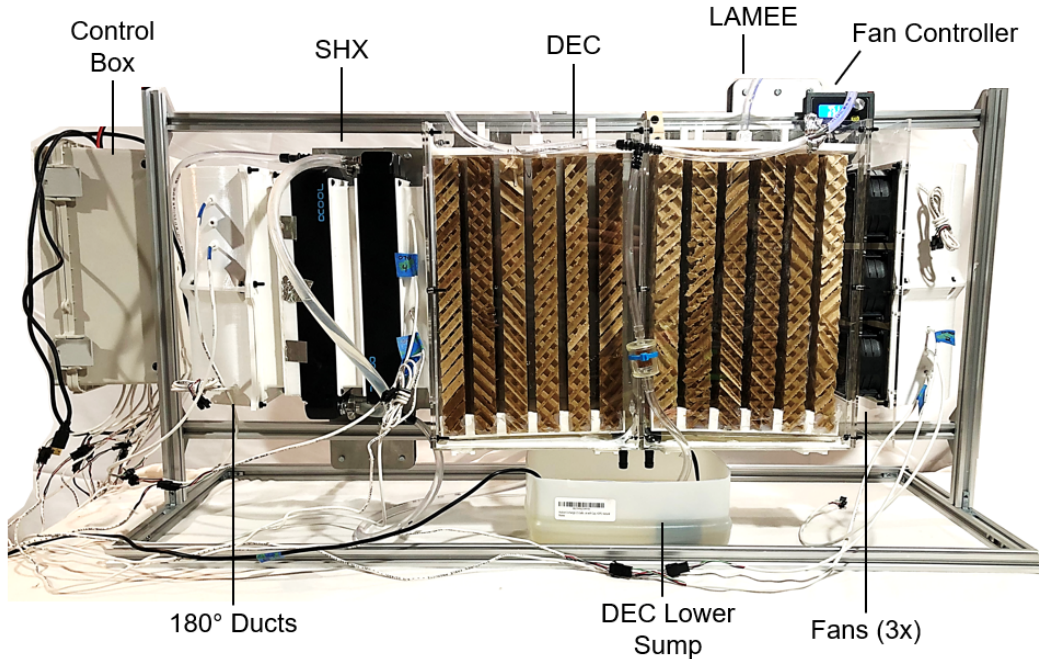
Figure 4-2: Benchtop Test Rig

module consists of two identical housings with evaporative media pads which share a water source. Each of the two housings consists of five clear acrylic panels with laser-cut openings and boltholes. The panels are acrylic welded in place and sealed at the bottom edge with silicone caulk to maintain a water-tight seal. The header forms a tight fit to the edges of the housing and forms the upper seal to contain the airflow. There is a small ($<$1mm) air gap between the top of the evaporative media pads and the header to ensure free water flow. The header is 3D printed in PLA. It is designed to be removable to allow easy access to the evaporative media for maintenance and repair. It is held in place by 4 mount hooks near the corners to position it in place directly above the media. Water is supplied through a nozzle on top and flows through printed-in channels to ensure even water distribution to each of the pads, four 2mm diameter holes supply each of the six pads. Figure 4-3 (left) shows the flow channel pattern.

The cooling pads consist of a wet durable paper formed into a corrugated pattern. The channels formed by corrugation are set at an angle (wave angle) to the incoming flow and alternate such that flow on one side is directed upward while the opposing

82

side is directed downward. A cooling pad for Honeywell C030XE is used in the test. This pad has a wave angle of 45 degrees on both sides. Most traditional DEC systems have small aspect ratios, i.e. the length in the flow direction is substantially less than the face area of the pad. The DECAL module requires a deep evaporative media section to achieve high wet bulb effectiveness. If a conventional pad were used, excessive blockage would be created by the flow channels running into the top and bottom of the module. To address this, the pad is cut into 25mm thick sections with a 10mm gap between each pad. This configuration has the additional benefit of enhancing mass transfer by repeatedly upsetting the boundary layer at each new pad. Figure 4-3 (right) shows the flow path of air through the pads.
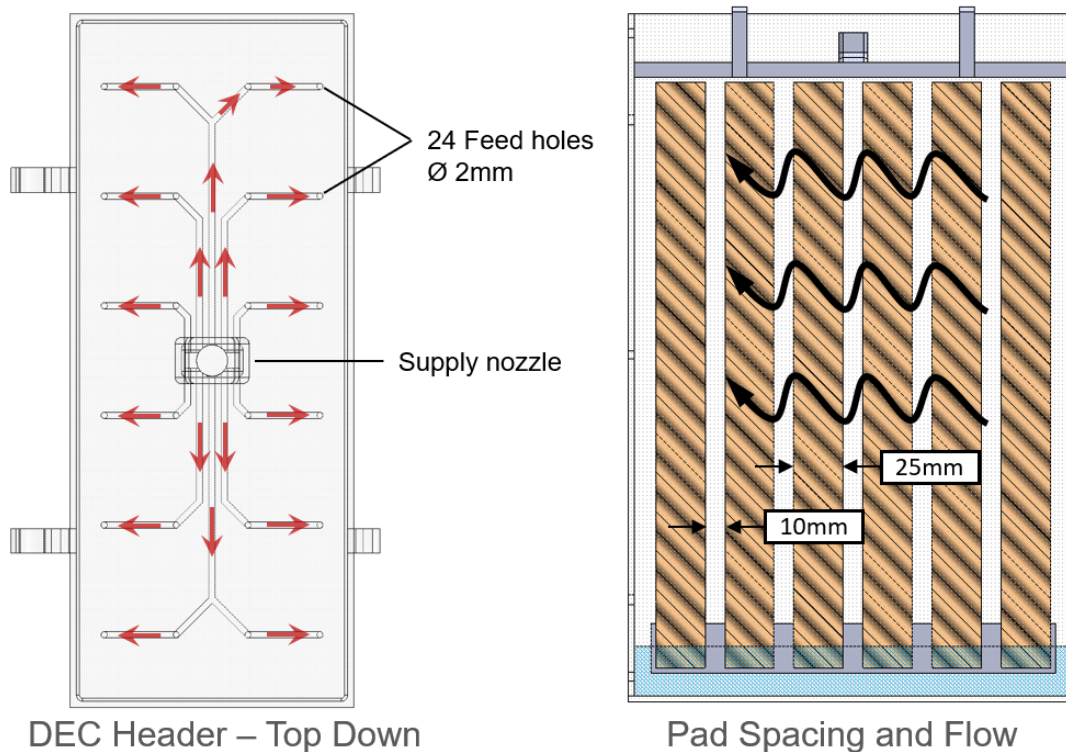

Figure 4-3: Direct Evaporative Cooler Module

The pads are held in place at uniform spacing by two 3d printed spacer rails glued to the bottom of the pads at the outside edge. The pad subassembly is friction fit into the housing to minimize leakage around the edges. The rails are suspended 15mm above the bottom of the vessel, resting on a pair of bumpers at each end. Water

collects in a sump (referred to as the upper sump) at the bottom of the housing, submerging the bottom of the pads and preventing air passage on the bottom side. A drain tube allows water to leave the housing once approximately 30mm of water has collected. Figure 4-4 shows the sub-assembly which makes up half of the DEC module.
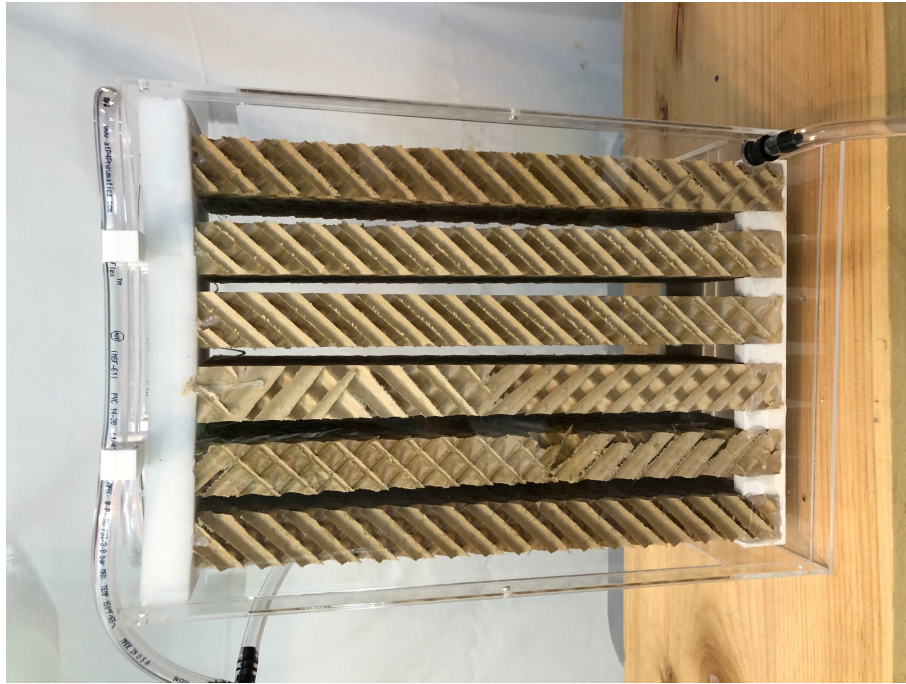

Figure 4-4: DEC Module Subassembly

Water flows from the upper sump of each housing to a shared lower sump directly below the module. A small 3W rotary vane pump returns flow from the lower sump to the headers, completing the circuit. Figure 4-5 (right) shows the flow circuit for the full DEC module.

4.2.2   SHX Module Design

The sensible heat exchanger module consists of two Alphacool NexXxoS XT45 water-to-air radiators. These are cross-flow heat exchangers with headers at the top and bottom of the unit. The heat exchanger has fins on the air side in a sinusoidal pattern with 2mm spacing between fins and 7.5mm channel height. The water-side channels are 2mm wide and run the full length of the unit. The two exchangers are arranged
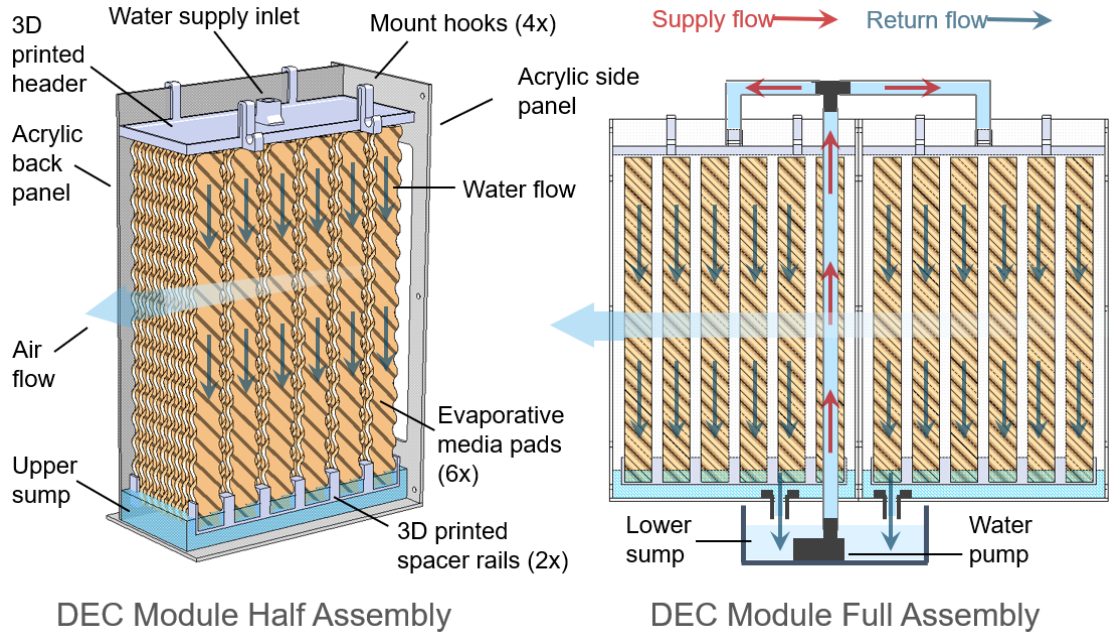
Figure 4-5: Direct Evaporative Cooler Module

in series with a 3D printed air duct between them and ducts on both ends which secure the module to the mating hardware. Heat exchange surfaces (fins and water manifolds) are copper. Water flows opposite the direction of airflow as shown in figure 4-6. This allows the overall thermal performance to exceed cross-flow effectiveness without extensive modifications to the hardware. Water flows to and from the module through 1/4" ID flexible vinyl tubing driven by a small rotary vane pump. The flow is metered upstream of the SHX with a metering valve and flow meter.

4.2.3   LAMEE Module Design

The LAMEE consists of 7 liquid desiccant layers, 8 air channel layers, a top plate, and a bottom plate stacked to form a parallel plate exchanger. Figure 4-7 shows the design of each layer. Each LD layer consists of a 2mm thick PETG LD flow plate, 2 3D printed manifold gates at the inlet and outlet header, and 2 sheets (top and bottom) of polypropylene membrane with 3um pores which allows water vapor transmittance between the LD and air. Liquid desiccant flows from the inlet header to the outlet header in each LD layer through a series of switchbacks formed by
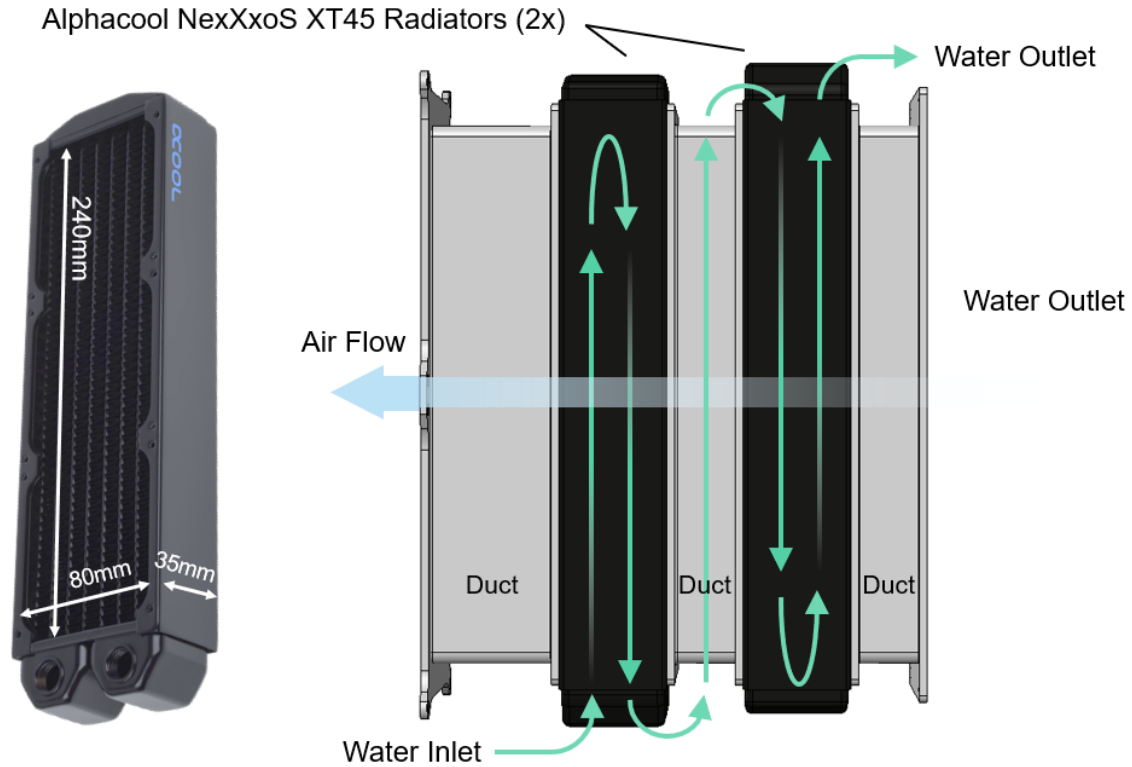
Figure 4-6: Sensible Heat Exchanger Module

interdigitating "fingers" protruding from the sides of the LD flow plate. The resulting smaller passages control the flow and ensure a uniform flow distribution from inlet to exit. Each of the 11 passes is normal to the air flow direction but results in a net counterflow effect. The manifold gates at inlet and outlet headers include small passages allowing LD to flow through the center while enabling a continuous seal (red line in figure 4-7) around the perimeter of the membrane. The membrane is fixed to the LD plate and sealed from the air flow layer by a thin foil tape around the perimeter of the plate. The air flow layer consists of two 2mm thick PETG plates forming the outer channel, and 5 air flow divider plates spaced evenly between them. Air flows straight through the channels in counterflow to the LD flow direction. When stacked, the interdigitating fingers of the LD plate and the air flow dividers overlap as shown in the figure, providing structural stability and preventing collapse of both channels with minimal sacrifice to exchange and flow area.
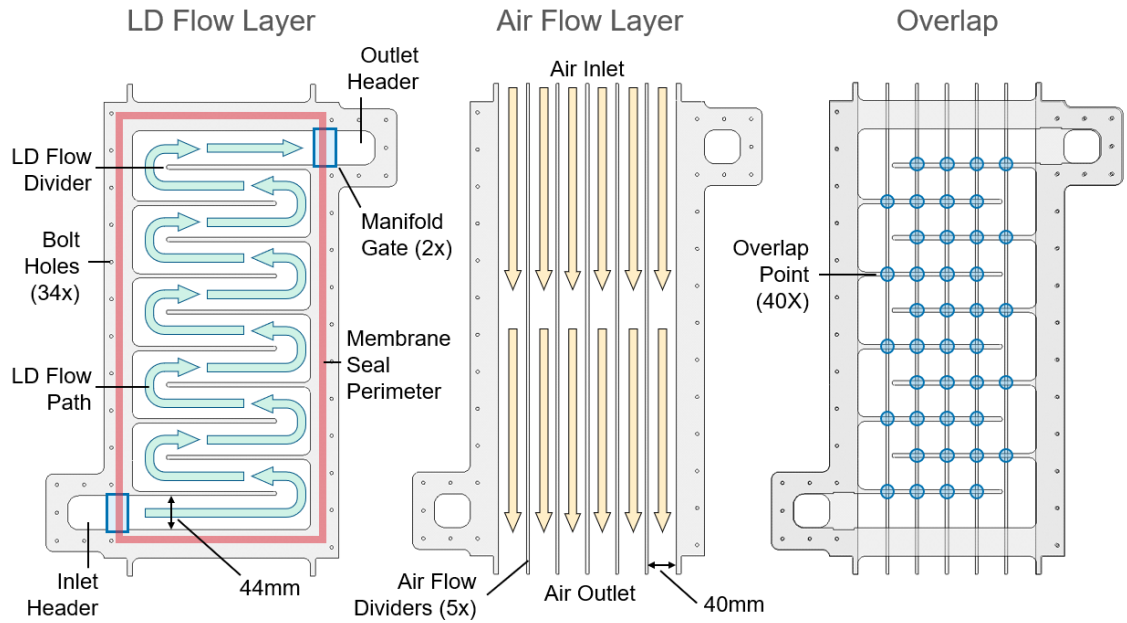
Figure 4-7: LAMEE Layers and Flow Pattern

4.2.4 Instrumentation

The test rig is instrumented to record temperature and relative humidity at each of the three control volumes in the process air loop (AP1-AP3), inlet and outlet water temperature from the SHX, reservoir temperature of the DEC, and inlet and outlet temperature of the liquid desiccant in the LAMEE. The relative humidity of the air in the LD supply and discharge tanks are also measured to estimate the mass concentration change of the LD stream. The pressure drop is also measured across each of the 3 exchangers, and airflow velocity is measured at the exit of the SHX. Table 4.2.4 gives the model of each sensor used in the test and accuracies at the relevant conditions.

| Sensor | Measurement | Range | | Accuracy |
		Min	Max	
Si7021A20	Temperature	-10C	85C	+/- 0.4C
Si7021A20	Humidity	0%	80%	+/- 3%
		80%	100%	+/- 5%
DS18S20	Temperature	-10C	85C	+/- 0.5C
MPL3115A2	Differential Pressure	50kPa	110kPa	+/- 1.5Pa
Testo 0560 1405 01	Air Velocity	0 m/s	2 m/s	+/- 0.1 m/s + 5%
		2 m/s	15 m/s	+/- 0.3 m/s + 5%

Figure 4-8 shows placement of each sensor in the test rig setup, as well as layout of the data collection system. Si7021 and MPL3115A2 sensors collect data and communicate via I2C to an Arduino Uno. Since the Uno has only a single I2C pin, two addressable TCA9548A multiplexers are required for the I2C sensors. The DS18S20 sensors output directly to the Uno via "onewire" digital signal.
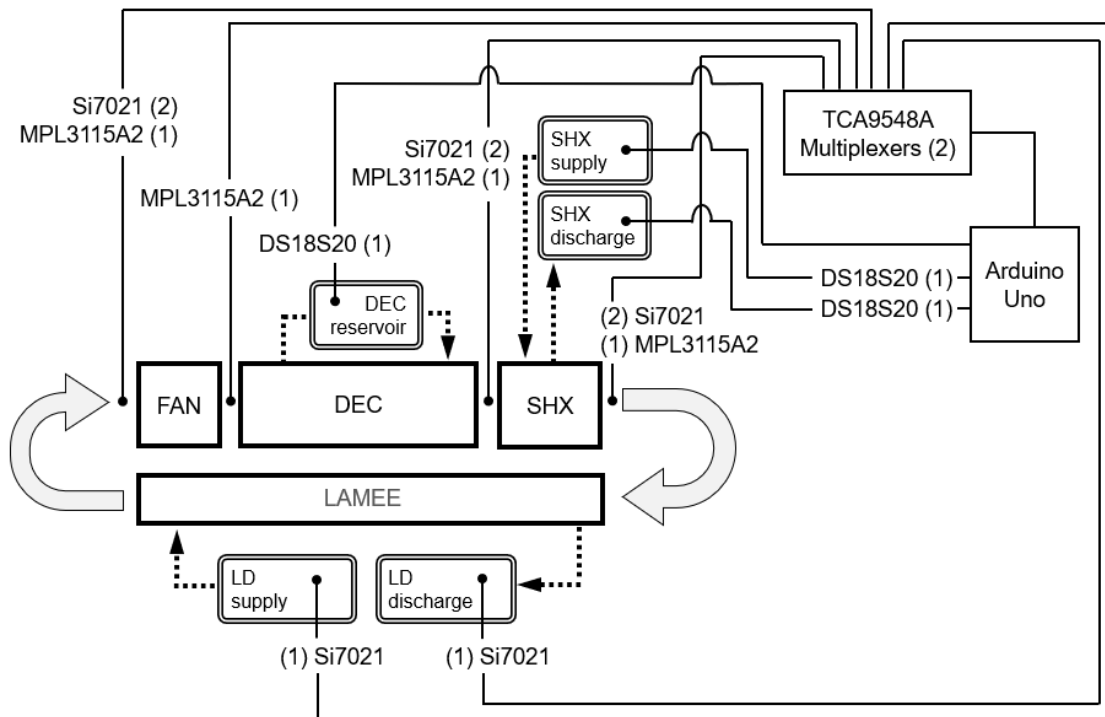

Figure 4-8: System Instrumentation Layout

Air sensors - (2x) Si7021 and (1x) MPL3115A2 - are placed at the center of the air stream in each of the two U-ducts (LAMEE inlet and exit) and the duct between the DEC and SHX. See figure 4-9 (left).
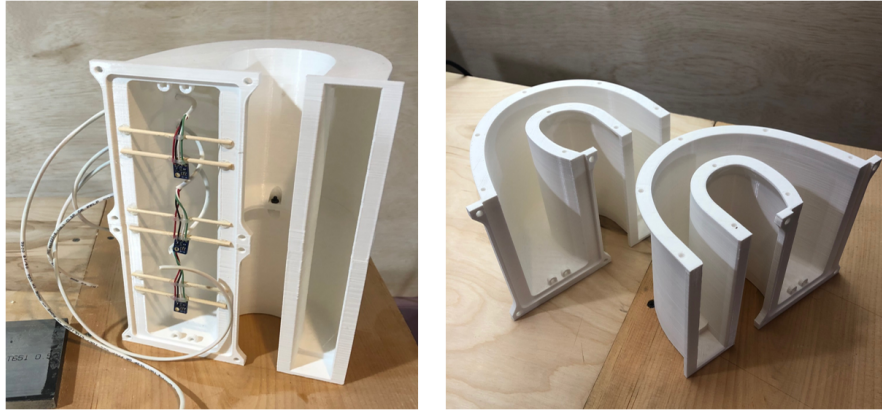
Figure 4-9: Left: Instrumented U-Duct Assembly Right: Split Ducts As-Printed

The U-Ducts exceeded the build volume of the 3D printer (270mm total height) and their geometry would not support printing as a single structure. Instead they were printed as a 2-part mirrored assembly and bolted together along a center-line flange as shown in figure 4-9 (right).

4.3   Testing

4.3.1   DEC Effectiveness Testing

The DEC module was tested to validate its wet bulb effectiveness and pressure drop characteristics against the mathematical model. Water was supplied from a small sump under the unit to the 3D printed headers and onto the evaporative media, then back to the sump and recirculated. Inlet and outlet temperature and relative humidity was measured. Fan speed was varied from 1 m/s to 5 m/s face velocity and the wet bulb effectiveness was calculated over the range of airflows. Results are shown in figure 4-10.

Here DEC effectiveness trends up with face velocity when it should trend down. This is likely due to thermal gain from the environment at low airflow rates coun-
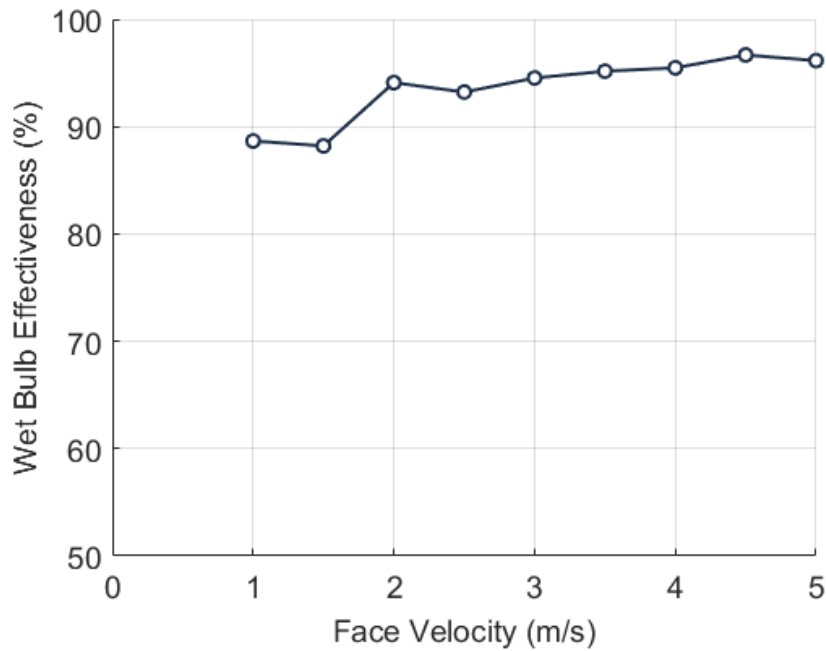
Figure 4-10: DEC Effectiveness vs Face Velocity

teracting the sensible cooling of the DEC. Relative humidity measurements indicate the air stream is fully saturated at the exit at lower airflows and begin to fall as face velocity increases (still over 95% with a +/- 5% error margin at this RH value).

4.3.2   SHX Effectiveness Testing

The sensible effectiveness of the SHX was tested to validate the model. The module was set up on a test stand with the fans pushing air through the heat exchangers and the anemometer measuring airflow velocity at the exit. A 3D printed flow straightener was used to ensure flow was fully developed and uniform to ensure proper volume flow calculations. The water was supplied from an ice bath to maximize the temperature gradient and improve the resolution of the test. Water flow rate was controlled by an upstream tapered bore variable area flow meter and metering valve. Air flow and water flow were varied together to maintain a constant Cr of 1, while sweeping SHX channel velocity from 1-3 m/s (corresponding to 26.2-78.6 CFM volume flow). Measured effectiveness is calculated from its definition (equation 4.1) based on the temperature change on the water side.

$$\varepsilon_{measured} = \frac{T_{H_2O\ out} - T_{H_2O\ in}}{T_{air\ in} - T_{H_2O\ in}} \tag{4.1}$$

Figure 4-11 shows the results of the test plotted against the effectiveness results from the model for counterflow and crossflow geometries. As expected, the measured effectiveness lies between these two bounds. Based on this result, the average between counterflow and crossflow effectiveness is used to predict performance on the benchtop test.
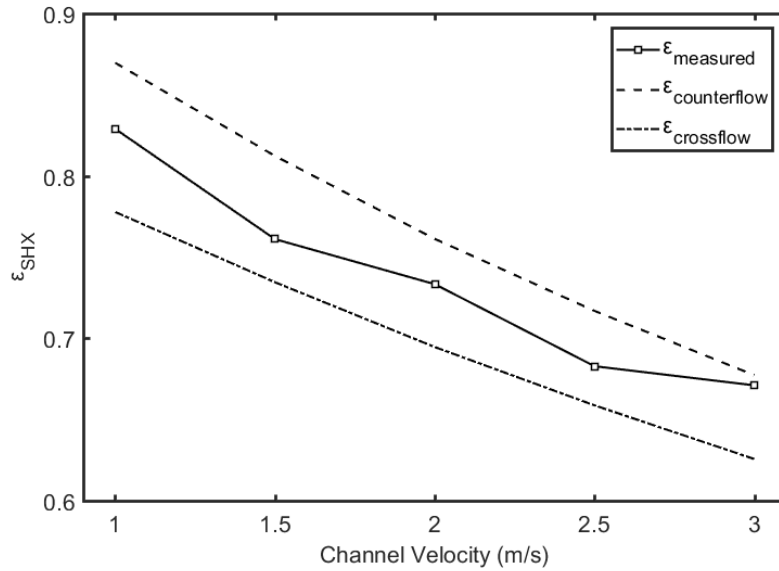
Figure 4-11: SHX Effectiveness vs Face Velocity

4.3.3   Full System Performance Testing

The full system was tested to demonstrate performance and validate the model predictions. Due to schedule constraints, only two full system tests were completed, first using $CaCl_2$ then using LiCl. Due to a data collection issue the CaCl test data was not recorded properly, so only the LiCl test point is presented here.

The LiCl test was run at a simulated condition consistent with the standard ambient conditions used elsewhere in this study: 35C dry bulb temperature and 60% RH. A process liquid desiccant supply temperature (LDP1) of 28.5C is used - consistent with a 95% wet bulb effectiveness on the reservoir DEC. Mass concentration

of the liquid desiccant is 0.33, and saturation concentration at 28.5C is 0.46, giving a concentration margin of 28%. The system was run at 20 CFM volume flow rate, and liquid desiccant and SHX water flow rates were set based on this flow to give a Cr of 1 for both the SHX and the LAMEE. The system was allowed to stabilize for 5 minutes after startup, and data was collected for 15 minutes. Over the recorded period temperature and RH measurements were stable, with less than 0.5C variation in temp and 5% variation in RH.

Experimental values for DEC wet bulb effectiveness, SHX sensible effectiveness, and LAMEE sensible effectiveness fit well with model pre-test predictions. LAMEE latent effectiveness was significantly lower than expected ($\varepsilon_{L\ predicted} = 0.97\ \varepsilon_{L\ measured} = 0.23$). The suspected root cause for this discrepancy is due to crystallization of $CaCl_2$ in the membrane pores between the fist and second tests. Ge [21] reports crystal blockage in membrane pores after regeneration, resulting in poor agreement between predicted and experimental latent effectiveness.

To account for this blockage, the membrane vapor diffusion resistance VDR is increased from 24 s/m to 800 s/m, resulting in a good fit between the model and experimental data. Figure 4-12 shows the process air cycle before and after R_{mem} adjustment and the experimental data. The reduction in latent effectiveness results in around 50% reduction in cooling power and 4.7C warmer cold air temperature in the cycle.

Further testing is recommended with new membranes. An effort should be made to source membranes with lower baseline VDR. Abdel-Salem [2] shows VDR varies widely in commercial membranes from 40-5793 s/m, so it is likely a higher-performance membrane could be used to further improve latent effectiveness.
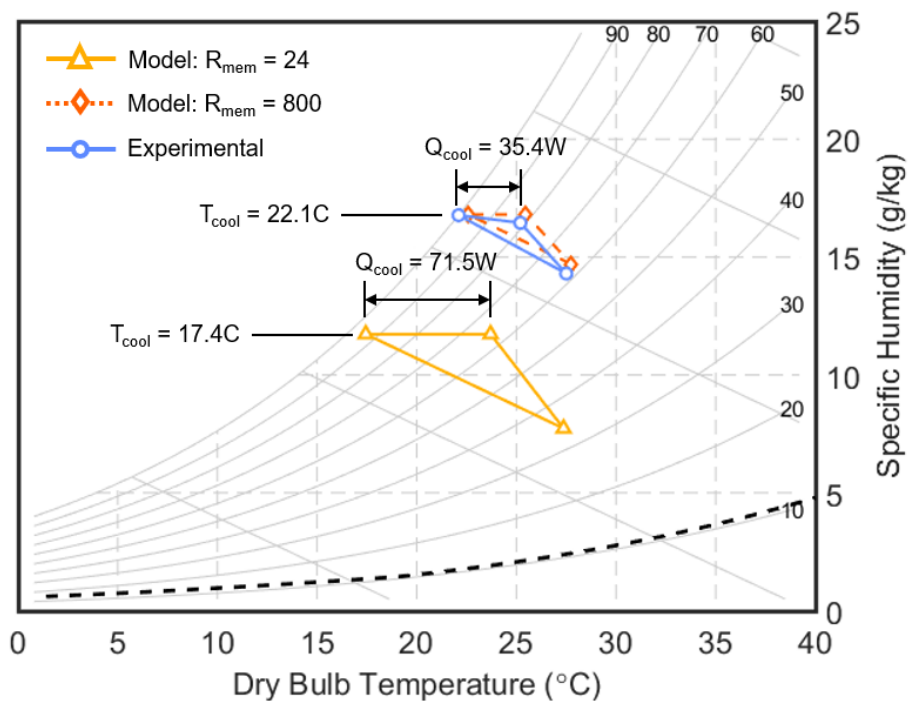
Figure 4-12: Full System Test Results

Chapter 5

Conclusions

The body of work in this thesis presents a novel approach to high efficiency air conditioning. The DECAL system is a liquid desiccant evaporative cooling cycle powered primarily by low-grade heat. Its key feature lies in the modularity of the system, which removes many of the integration challenges other LDACs face. DECAL aims to help offset the growing problem of energy demand for space cooling in the face of climate change.

Mathematical model results show DECAL holds great promise to enable high efficiency evaporative cooling in climates which previously would not support it. High thermal efficiency and low regeneration temperatures enable the use of waste heat to drive the cycle. The modular design requiring only liquid desiccant lines between modules makes the system attractive in many applications where direct air exchange systems are not viable.

Experimental testing shows that the overall cycle is feasible - i.e. a net cooling effect may be generated in a closed air system. When combined with a pre-cooling outdoor direct evaporative cooling system this enables cooling beyond the ambient wet-bulb temperature. Further experimental work is needed to prove out system performance. CaCl appears to have crystallized in the LAMEE membrane pores, greatly increasing the membrane resistance and reducing latent effectiveness significantly. Pore crystallization presents a significant challenge to the design of LDAC systems and should be explored in more depth in future studies. The heat exchanger effective-

ness should be improved - much higher performance HVAC radiators are available and could improve the heat transfer to pressure drop characteristics of the SHX. It may also be feasible to circulate the DEC reservoir water directly and use that stream for heat exchange rather than the air-water SHX presented here. This could potentially improve efficiency and reduce system size.

5.1   Lessons Learned

This section details a few of the many lessons learned from the experimental work of this thesis. It is intended to aid future researchers conducting experimental studies in this field.

Special care should be taken from the beginning to ensure exchanger form factor gives an optimal balance between pressure drop and exchanger effectiveness. The extreme uncertainty and unconventional nature of testing for this project due to Covid19 led to a somewhat ad hoc approach which resulted in further challenges down the line. The LAMEE design was based on a total surface area requirement and the perception that risk of leakage would be reduced if fewer plates were used. In hindsight, a design with more layers (15-25) and larger face area would have significantly reduced pressure drop in the LAMEE and allowed greater mass flow. This would have not only improved system electrical COP, but also relieved some of the challenges encountered in collecting reliable data associated with low flow rates.

Volume flow on the liquid side was reduced with airflow to keep a capacitance ratio of 1. This created challenges measuring volume flow of the liquid streams - both controlled by a metering valve on a tapered bore float meter. The reduced flows were near the bottom of the scale and resolution was course. Higher quality flow meters and pumps should be used once the system can be measured in the lab.

Vapor lock led to significant challenges in testing. Future designs should pay close attention to positioning of pumps, tanks, flow meters, and exchangers to minimize potential air traps and incorporate vent valves if necessary. It is recommended to purge the system with water or LD and use valves to prevent air entering the system.

The DEC was designed to allow standing water at the bottom to prevent air flowing under the evaporative media plates. The design worked, but the upstream water level reduces with air pressure. At high enough pressure this would allow flow under the first layer of evaporative media. The pads should be designed to reach the bottom of the sump to prevent this.

5.2 Future Work

The following studies are recommended as next steps in development of the DECAL system.

- Techno-economic analysis of DECAL system to assess viability in terms of production costs, payback period, etc.

- A comprehensive study on conditions which lead to LD crystallization in pores. Including operating conditions as well as rinse and flush procedures before and after operation to avoid crystallization.

- More thorough of testing in the lab with improved instrumentation and a more controlled environment. Specific attention should be given to measurement of mass flow of the air and fluid flow streams.

- Replace the top plate of the LAMEE with a thick acrylic plate to allow visual inspection of the LD flow during operation, perhaps using a dye tracer to visualize flow.

- Further development of the regeneration system using solar thermal collector or a waste heat source.

Appendix A

Tables

Brand	Outdoor Unit Model	Ht (in)	Wd(in)	Dp (in)	Vol (in3)	Indoor Unit Model	Ht (in)	Wd (in)	Dp (in)	Vol (in3)	cc/W	Capacity (kW)	COP	SEER
Fujitsu	AOU9RLFF	24.4	31.1	11.4	8700	AGU9RLF	23.6	29.1	7.9	5419	87.7	2.64	4.69	7.62
Fujitsu	AOU9RLFC	24.5	31.1	11.3	8642	AUU9RLF	9.7	22.4	22.4	4877	84.0	2.64	4.25	7.03
Fujitsu	AOU12RLFF	24.4	31.1	11.4	8700	AGU12RLF	23.6	29.1	7.9	5419	65.8	3.52	3.84	6.65
Fujitsu	AOU12RLFC	24.5	31.1	11.3	8628	ARU12RLF	7.8	27.6	24.4	5262	64.7	3.52	3.75	5.86
Fujitsu	AOU12RLFC	24.5	31.1	11.3	8642	AUU12RLF	9.7	22.4	22.4	4877	63.0	3.52	3.75	6.42
Fujitsu	AOU15RLFF	24.4	31.1	11.4	8700	AGU15RLF	23.6	29.1	7.9	5419	55.6	4.16	3.66	5.95
Fujitsu	AOU12RLFW1	21.3	31.1	11.4	7565	ASU12RLF1	10.5	33.1	8.0	2783	48.2	3.52	3.66	6.45
Fujitsu	AOU18RLXFZH	32.7	35.4	13.0	15059	Non-ducted	0.0	0.0	0.0	0	46.8	5.28	3.96	6.30
Fujitsu	AOU24RLXFZH	32.7	35.4	13.0	15059	Non-ducted	0.0	0.0	0.0	0	38.3	6.45	3.90	5.86
Fujitsu	AOU36RLXFZH	39.3	38.2	14.6	21862	Non-ducted	0.0	0.0	0.0	0	34.7	10.32	3.81	5.86
LG	LAU240HYV1	31.5	38.3	14.2	17122	LAN240HYV1	13.0	42.9	9.8	5457	57.4	6.45	3.66	6.45
LG	LAU120HYV1	21.5	30.3	11.3	7373	LAN120HYV1	11.6	34.4	9.3	3703	56.3	3.22	4.04	7.47
Mitsubishi	MUZ-FH06NA	21.6	31.5	11.3	7663	MSZ-FH06NA**	12.7	36.4	9.2	4247	111.0	1.76	5.57	9.70
Mitsubishi	PUZ-A12NKA7***	25.0	32.0	11.0	8800	PLA-A12EA*	33.1	33.1	10.2	11102	92.7	3.52	4.81	7.91
Mitsubishi	PUY-A12NKA7***	25.0	32.0	11.0	8800	PLA-A12EA*	33.1	33.1	10.2	11102	92.7	3.52	4.81	7.91
Mitsubishi	PUZ-A24NKA7***	37.1	37.5	14.0	19491	PLA-A24EA*	33.1	33.1	11.8	12844	75.3	7.03	4.19	7.09
Mitsubishi	PUY-A24NHA7***	37.1	37.5	14.0	19491	PLA-A24EA*	33.1	33.1	11.8	12844	75.3	7.03	4.19	7.09
Mitsubishi	MUZ-FH09NA	21.6	31.5	11.3	7663	MSZ-FH09NA	12.7	36.4	9.2	4247	74.0	2.64	4.72	8.94
Mitsubishi	MUZ-FH15NA	34.6	33.1	13.0	14882	MSZ-FH15NA	12.7	36.4	9.2	4247	71.3	4.40	3.66	6.45
Mitsubishi	MUZ-GL09NA-U8	21.6	31.5	11.3	7663	MSZ-GL09NA-U1	11.6	31.4	9.1	3335	68.3	2.64	4.51	7.21
Mitsubishi	MUY-GL09NA-U1	21.6	31.5	11.3	7663	MSY-GL09NA-U1	11.6	31.4	9.1	3335	68.3	2.64	4.51	7.21
Mitsubishi	PUZ-A36NKA7***	52.8	41.2	14.0	30432	PLA-A36EA*	11.8	33.1	33.1	12844	67.2	10.55	3.78	6.39
Mitsubishi	PUY-A36NKA7***	52.8	41.2	14.0	30432	PLA-A36EA*	11.8	33.1	33.1	12844	67.2	10.55	3.78	6.39
Mitsubishi	MUZ-FH18NA2	34.6	33.1	13.0	14882	MSZ-FH18NA**	12.8	36.8	9.4	4414	62.7	5.04	3.66	6.15
Mitsubishi	PUZ-A18NKA7***	25.0	32.0	11.0	8800	PLA-A18EA*	10.1	33.1	33.1	11091	61.8	5.28	4.22	7.21
Mitsubishi	PUY-A18NKA7***	25.0	32.0	11.0	8800	PLA-A18EA*	10.1	33.1	33.1	11091	61.8	5.28	4.22	7.21
Mitsubishi	MUZ-GL18NA-U1	34.6	33.1	13.0	14910	MSZ-GL18NA-U1	12.0	36.3	9.8	4276	59.6	5.28	3.93	6.01
Mitsubishi	MUY-GL18NA-U1	34.6	33.1	13.0	14910	MSY-GL18NA-U1	12.0	36.3	9.8	4276	59.6	5.28	3.93	6.01
Mitsubishi	MUZ-FH12NA	21.6	31.5	11.3	7663	MSZ-FH12NA	12.7	36.4	9.2	4247	55.5	3.52	4.04	7.65
Mitsubishi	MUZ-GL12NA-U1	21.6	31.5	11.3	7663	MSZ-GL12NA-U1	11.6	31.4	9.1	3335	51.2	3.52	3.81	6.77
Mitsubishi	MUY-GL12NA-U1	21.6	31.5	11.3	7663	MSY-GL12NA-U1	11.6	31.4	9.1	3335	51.2	3.52	3.81	6.77
Mitsubishi	MUZ-GL24NA-U1	34.6	33.1	13.0	14910	MSZ-GL24NA-U1	12.8	43.3	9.4	5203	50.2	6.56	3.66	6.01
Mitsubishi	MUY-GL24NA-U1	34.6	33.1	13.0	14910	MSY-GL24NA-U1	12.8	43.3	9.4	5203	50.2	6.56	3.66	6.01
Mitsubishi	MUZ-GL15NA-U1	21.6	31.5	11.3	7663	MSZ-GL15NA-U1	11.6	31.4	9.1	3335	43.9	4.10	3.81	6.33
Mitsubishi	MUY-GL15NA-U1	21.6	31.5	11.3	7663	MSY-GL15NA-U1	11.6	31.4	9.1	3335	43.9	4.10	3.81	6.33

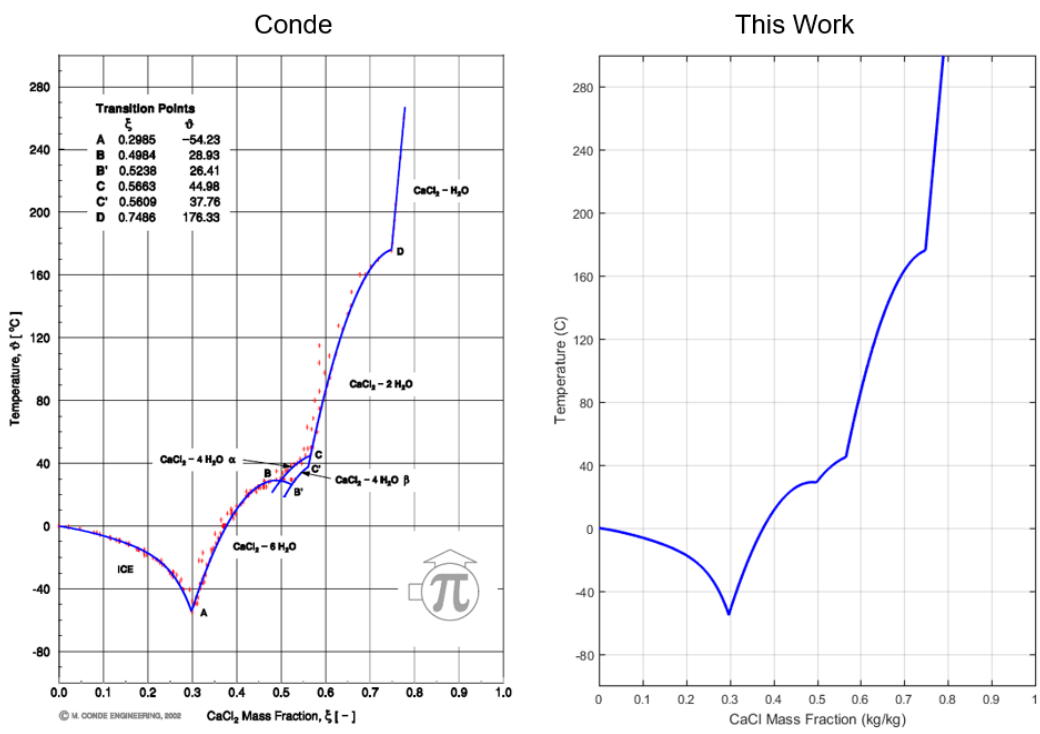Table A.1: Energy Star Rated Mini-Split AC Data

Appendix B

Figures

Figure B-1: Liquid Desiccant State Calculations - CaCl$_2$ Solubility Limit Validation
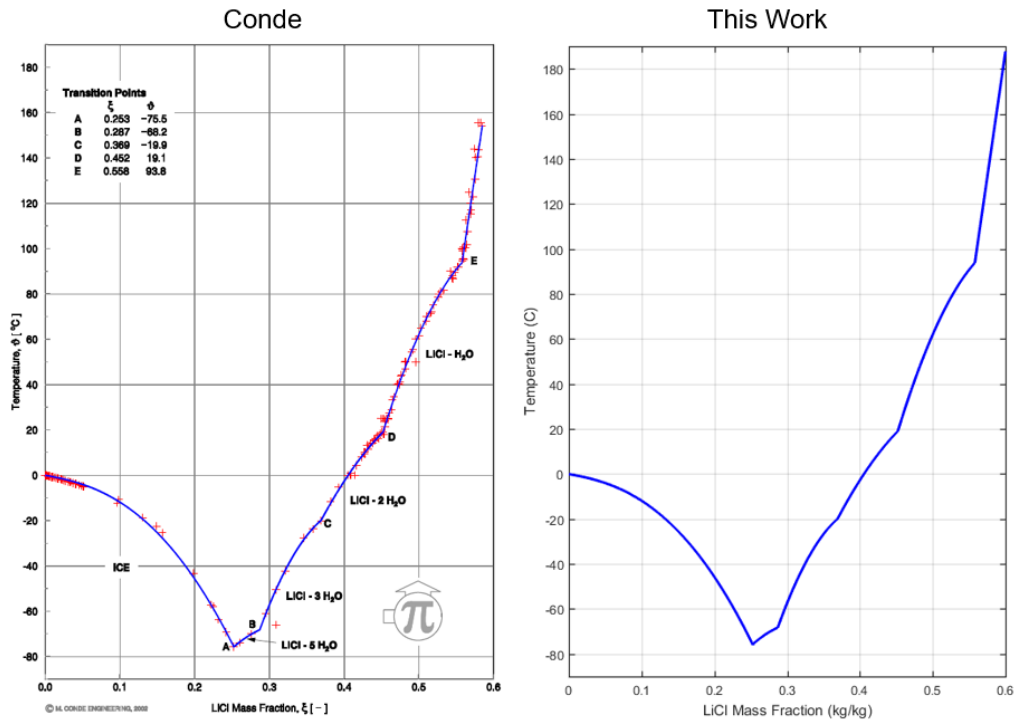
Figure B-2: Liquid Desiccant State Calculations - LiCl Solubility Limit Validation
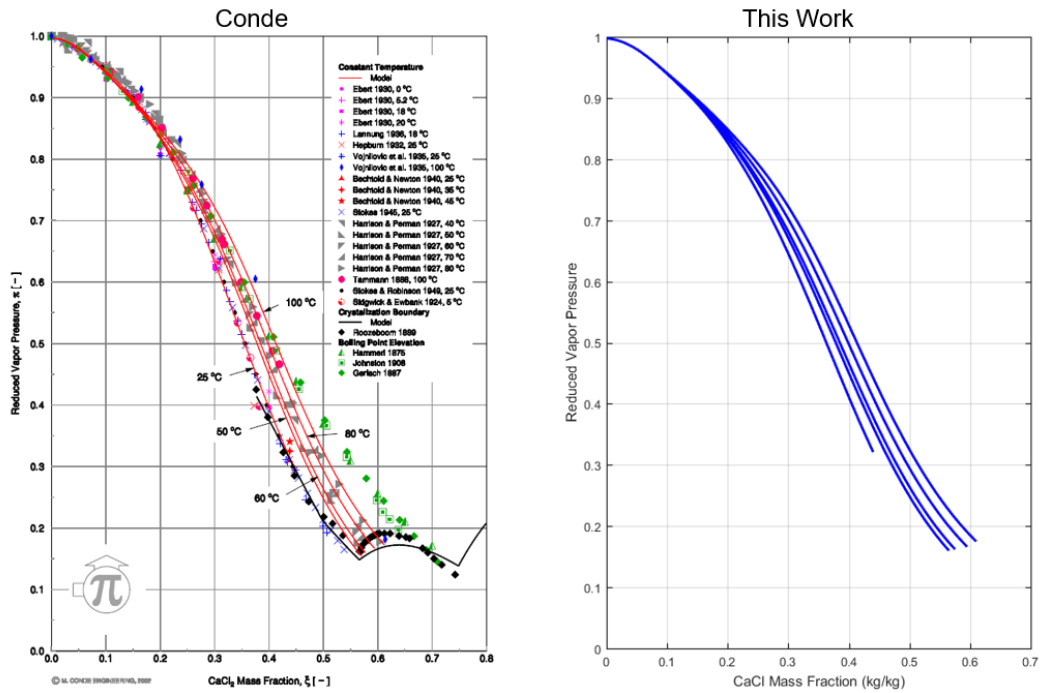

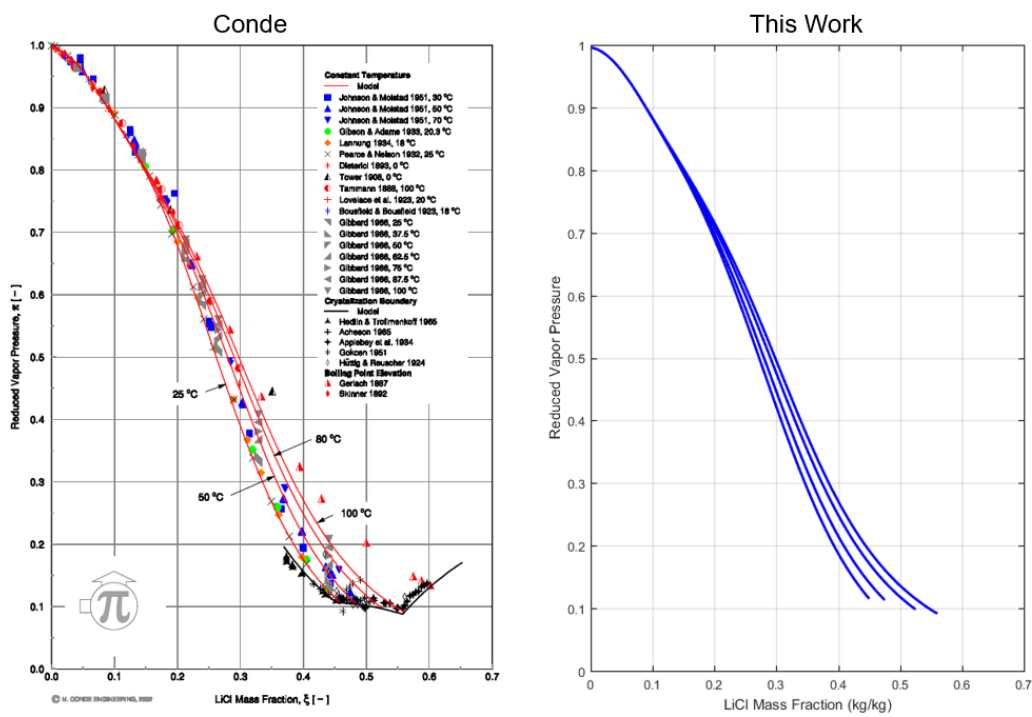Figure B-3: Liquid Desiccant State Calculations - CaCl$_2$ Vapor Pressure Validation

Figure B-4: Liquid Desiccant State Calculations - LiCl Vapor Pressure Validation

Bibliography

[1] Ahmed H Abdel-Salam, Gaoming Ge, and Carey J Simonson. Thermo-economic performance of a solar membrane liquid desiccant air conditioning system. *Solar Energy*, 102:56–73, 2014.

[2] Mohamed RH Abdel-Salam, Gaoming Ge, Melanie Fauchoux, Robert W Besant, and Carey J Simonson. State-of-the-art in liquid-to-air membrane energy exchangers (lamees): A comprehensive review. *Renewable and Sustainable Energy Reviews*, 39:700–728, 2014.

[3] IEA (International Energy Agency). The future of cooling. opportunities for energy efficient air conditioning, 2018.

[4] International Energy Agency. *World Energy Outlook 2019*. International Energy Agency, 2019.

[5] Refrigeration American Society of Heating and Air-Conditioning Engineers. *2017 ASHRAE Handbook Funadamentals*. ASHRAE, 2017.

[6] Hongyu Bai, Jie Zhu, Ziwei Chen, Lina Ma, Ruzhu Wang, and Tingxian Li. Performance testing of a cross-flow membrane-based liquid desiccant dehumidification system. *Applied Thermal Engineering*, 119:119–131, 2017.

[7] The World Bank. GDP per capita (current US$), 2020. https://data.worldbank.org/indicator/NY.GDP.PCAP.CD?view=chart.

[8] Hilmi Cenk Bayrakçi and Arif Emre Özgür. Energy and exergy analysis of vapor compression refrigeration system using pure hydrocarbon refrigerants. *International Journal of Energy Research*, 33(12):1070–1075, 2009.

[9] Hüseyin Benli. A performance comparison between a horizontal source and a vertical source heat pump systems for a greenhouse heating in the mild climate elaziğ, turkey. *Applied Thermal Engineering*, 50(1):197–206, 2013.

[10] Theodore L. Bergman, Adrienne S. Lavine, Frank P. Incropera, and David P. Dewitt. *Fundamentals of Heat and Mass Transfer, Seventh Edition*, chapter 1.1. Wiley, 2011.

[11] A Beshkani and REZA Hosseini. Numerical modeling of rigid media evaporative cooler. *Applied thermal engineering*, 26(5-6):636–643, 2006.

[12] E Bilgen and H Takahashi. Exergy analysis and experimental study of heat pump systems. *Exergy, an international journal*, 2(4):259–265, 2002.

[13] Yunus Cengel and Michael Boles. *Thermodynamics : an engineering approach*. McGraw-Hill Higher Education, Boston, 2008.

[14] Qing Cheng and Wenhao Xu. Performance analysis of a novel multi-function liquid desiccant regeneration system for liquid desiccant air-conditioning system. *Energy*, 140:240–252, 2017.

[15] Manuel R Conde-Petit. Aqueous solutions of lithium and calcium chlorides:-property formulations for use in air conditioning equipment design. *Zurich, Switzerland*, 2014.

[16] by Seeley International Coolerado. Coolerado m50c 1ph submittal data sheet.

[17] Huabo Duan, T Reed Miller, Gang Liu, Xianlai Zeng, Keli Yu, Qifei Huang, Jian Zuo, Yufei Qin, and Jinhui Li. Chilling prospect: climate change effects of mismanaged refrigerants in china. *Environmental science & technology*, 52(11):6350–6356, 2018.

[18] EPA. International treaties and cooperation about the protection of the stratospheric ozone layer, Sep 2018.

[19] Georgios Florides and Soteris Kalogirou. Ground heat exchangers—a review of systems, models and applications. *Renewable energy*, 32(15):2461–2478, 2007.

[20] Robert Fox. *Fox and McDonald's introduction to fluid mechanics*. John Wiley & Sons, Inc. John Wiley distributor, Hoboken, NJ Chichester, 2011.

[21] Gaoming Ge, Davood Ghadiri Moghaddam, Ahmed H Abdel-Salam, Robert W Besant, and Carey J Simonson. Comparison of experimental data and a model for heat and mass transfer performance of a liquid-to-air membrane energy exchanger (lamee) when used for air dehumidification and salt solution regeneration. *International Journal of Heat and Mass Transfer*, 68:119–131, 2014.

[22] Gaoming Ge, Davood Ghadiri Moghaddam, Ramin Namvar, Carey J Simonson, and Robert W Besant. Analytical model based performance evaluation, sizing and coupling flow optimization of liquid desiccant run-around membrane energy exchanger systems. *Energy and buildings*, 62:248–257, 2013.

[23] Gabriel Happle, Erik Wilhelm, Jimeno A. Fonseca, and Arno Schlueter. Determining air-conditioning usage patterns in singapore from distributed, portable sensors. *Energy Procedia*, 122(2017):313–318, 2017.

[24] Lewis Harriman. *The dehumidification handbook*. Munters Corporation, Amesbury, MA, 2002.

[25] Intergovernmental Panel On Climate Change IPCC. Special report on global warming of 1.5 c (sr15), 2019.

[26] DB Jani, Manish Mishra, and PK Sahoo. Solid desiccant air conditioning–a state of the art review. *Renewable and Sustainable Energy Reviews*, 60:1451–1469, 2016.

[27] Miklos Kassai, Gaoming Ge, and Carey J Simonson. Dehumidification performance investigation of run-around membrane energy exchanger system. *Thermal Science*, 20(6):1927–1938, 2016.

[28] Eric Kozubal, Jason Woods, Jay Burch, Aaron Boranian, and Tim Merrigan. Desiccant enhanced evaporative air-conditioning (devap): evaluation of a new concept in ultra efficient air conditioning. Technical report, National Renewable Energy Lab.(NREL), Golden, CO (United States), 2011.

[29] Y Siva Kumar Reddy, Karthik Balasubramanian, and VP Chandramohan. Influence of potential liquid desiccants on solution cooling, heating, and pumping loads of membrane-based liquid desiccant air conditioning system: An analytical study. *Science and Technology for the Built Environment*, 25(6):753–766, 2019.

[30] Zengwen Li, Hongxia Zhao, Jitian Han, Xinli Wang, and Jie Zhu. Performance optimization of the dehumidifier with parallel-plate membrane modules. *Energy*, 194:116829, 2020.

[31] Su Liu and Jae-Weon Jeong. Energy performance comparison between two liquid desiccant and evaporative cooling-assisted air conditioning systems. *Energies*, 13(3):522, 2020.

[32] Abdollah Malli, Hamid Reza Seyf, Mohammad Layeghi, Seyedmehdi Sharifian, and Hamid Behravesh. Investigating the performance of cellulosic evaporative cooling pads. *Energy Conversion and Management*, 52(7):2598–2603, 2011.

[33] G. Myhre, D. Shindell, F.-M. Breon, W. Collins, J. Fuglestvedt, J. Huang, D. Koch, J.-F. Lamarque, D. Lee, B. Mendoza, T. Nakajima, A. Robock, G. Stephens, T. Takemura, and H. Zhang. Anthropogenic and natural radiative forcing. In T.F. Stocker, D. Qin, G.-K. Plattner, M. Tignor, S.K. Allen, J. Boschung, A. Nauels, Y. Xia, V. Bex, and P.M. Midgley, editors, *Climate Change 2013: The Physical Science Basis. Contribution of Working Group I to the Fifth Assessment Report of the Intergovernmental Panel on Climate Change*, page 659–740, Cambridge, United Kingdom and New York, NY, USA, 2013. Cambridge University Press.

[34] Ramin Namvar, Dave Pyra, Gaoming Ge, Carey J Simonson, and Robert W Besant. Transient characteristics of a liquid-to-air membrane energy exchanger (lamee) experimental data with correlations. *International journal of heat and mass transfer*, 55(23-24):6682–6694, 2012.

[35] UNDESA (United Nations Department of Economic and Social Affairs). World population prospects 2019, 2020. https://population.un.org/wpp/Download/Standard/Population/.

[36] Global Cooling Prize. The solution.

[37] B Riangvilaikul and S Kumar. An experimental study of a novel dew point evaporative cooling system. *Energy and Buildings*, 42(5):637–644, 2010.

[38] Ioan Sarbu and Calin Sebarchievici. General review of ground-source heat pump systems for heating and cooling of buildings. *Energy and buildings*, 70:441–454, 2014.

[39] RK Shah. A correlation for laminar hydrodynamic entry length solutions for circular and noncircular ducts. *Journal of Fluids Engineering*, 1978.

[40] Chenguang Sheng and AG Agwu Nnanna. Empirical correlation of cooling efficiency and transport phenomena of direct evaporative cooler. In *ASME International Mechanical Engineering Congress and Exposition*, volume 54907, pages 953–967, 2011.

[41] Energy Star. Energy star most efficient 2020, Jan 2020.

[42] Li Wang, Nianping Li, and Binwen Zhao. Exergy performance and thermodynamic properties of the ideal liquid desiccant dehumidification system. *Energy and buildings*, 42(12):2437–2444, 2010.

[43] JM Wu, X Huang, and H Zhang. Theoretical analysis on heat and mass transfer in a direct evaporative cooler. *Applied Thermal Engineering*, 29(5-6):980–984, 2009.

[44] ZQ Xiong, YJ Dai, and RZ Wang. Development of a novel two-stage liquid desiccant dehumidification system assisted by cacl2 solution using exergy analysis method. *Applied Energy*, 87(5):1495–1504, 2010.

[45] Bo Yang, Weixing Yuan, Feng Gao, and Binghan Guo. A review of membrane-based air dehumidification. *Indoor and Built Environment*, 24(1):11–26, 2015.